Received: 1 August 2022 | Revised: 13 December 2022 | Accepted: 6 March 2023

DOI: 10.1002/cac2.12414

CANCER COMMUNICATIONS Open Access

ORIGINAL ARTICLE

Cancer-associated fibroblast-derived secreted phosphoprotein 1 contributes to resistance of hepatocellular carcinoma to sorafenib and lenvatinib

Jung Woo Eun[1] | **Jung Hwan Yoon**[2] | **Hye Ri Ahn**[1,3] | **Seokhwi Kim**[4] | **Young Bae Kim**[4] | **Su Bin Lim**[5] | **Won Park**[6] | **Tae Wook Kang**[6] | **Geum Ok Baek**[1] | **Moon Gyeong Yoon**[1] | **Ju A Son**[1,3] | **Ji Hyang Weon**[1,3] | **Soon Sun Kim**[1] | **Hyo Jung Cho**[1] | **Jae Youn Cheong**[1]

List of abbreviations: α-SMA, alpha smooth muscle actin; AFP, alpha-fetoprotein; AKT, protein kinase B; ANOVA, one-way analysis of variance; avHCC, advanced HCC; BCLC, Barcelona Clinic Liver Cancer; Bcl2, B-cell lymphoma 2; BiNGO, Biological Networks Gene Oncology tool; BioGRID, The Biological General Repository for Interaction Datasets; BRAF, v-Raf murine sarcoma viral oncogene homolog B; BrdU, 5-bromo-2'-deoxyuridine-5'-monophosphate; CAFs, cancer-associated fibroblasts; Casp3, caspase3; Catholic LIHC, Catholic University of Korea's liver hepatocellular carcinoma project; c-Casp3, cleaved caspase3; CCLE, Cancer Cell Line Encyclopedia; CCL26, chemokine (C-C motif) ligand 26; cDC, classic dendritic cell; CH, chronic hepatitis; CI, confidence interval; CM, culture medium; co-IP, co-immunoprecipitation; COMP, cartilage oligomeric matrix protein; c-PARP, cleaved poly (ADP-ribose) polymerase; CT, computed tomography; CTGF, connective tissue growth factor; Ctrl, control; DAPI4′, 4′6-diamidino-2-phenylindole; DFS, disease free survival; DMEM, Dulbecco's modified eagle medium; DMSO, dimethyl sulfoxide; ECOG, eastern cooperative oncology group; eHCC, early HCC; ELISA, enzyme linked immunosorbent assay; EMT, epithelial mesenchymal transition; ERK, extracellular signal-related kinase; FAM3C, family with sequence similarity 3; FAP, fibroblast activation protein alpha; FDR, false discovery rate; FDR, false discovery rate; FGF, fibroblast growth factor; GAPDH, glyceraldehyde 3-phosphate dehydrogenase; GeneMANIA, gene multiple association network integration algorithm; GEO, Gene Expression Omnibus; GSEA, Gene Set Enrichment Analysis; H&E, hematoxylin and eosin; HCC, hepatocellular carcinoma; Hep3B-R, Hep3B-resistance cells; HR, hazard ratio; Huh-7-R, Huh-7-resitance cells; IB, immunoblotting; IC_{50}, half maximal inhibitory concentration; ICI, immune checkpoint inhibitor; IF, immunofluorescence; IgG, immunoglobulin G; IHC, immunohistochemistry; ITGA4, integrin subunit α4; ITGA5, integrin subunit α5; ITGA8, integrin subunit α8; ITGA9, integrin subunit α9; ITGAV, integrin subunit αV; ITGB1, integrin subunit β1; ITGB3, integrin subunit β3; ITGB5, integrin subunit β5; KRAS, Kirsten rat sarcoma virus; LC, liver cirrhosis; Len, lenvatinib;; LSEC, liver sinusoidal endothelial cell; LVEC, non-tumor liver vascular endothelial cell; LVECt, tumor liver vascular endothelial cell; MAPK, mitogen-activated protein kinase; MR, magnetic resonance; MSigDB, the Molecular Signatures Database; mTOR, mammalian target of rapamycin; mUICC, modified Union for International Cancer Control; NCBI, National Center for Biotechnology Information; NF, normal fibroblast; NL, normal liver; NOV, nephroblastoma overexpressed gene; NT, non-tumor; NTF3, neurotrophin-3; NTM, neurotrimin; OS, overall survival; PAF, para-cancer fibroblast; PARP, poly (ADP-ribose) polymerase; PBS, phosphate buffered saline; PCA, principal component analysis; PD, progressive disease; PFS, progression free survival; PI3K, phosphatidylinositol-3-kinase; PKCα, protein kinase C α; PR, partial response; qRT-PCR, quantitative reverse transcription polymerase chain reaction; RAF, rapidly accelerated fibrosarcoma; RBPs, receptor-binding proteins; RECIST, response evaluation criteria in solid tumors; RFU, relative fluorescence units; RSEM, RNA-Seq by Expectation-Maximization; rSPP1, recombinant SPP1; RTK, receptor tyrosine kinase; S, tumor stroma; SAMs, scar-associated macrophages; SD, stable disease; SEM, standard error of the mean; siCtrl, negative control; siRNA, small interfering RNA; SNN, shared nearest neighbor; Sor, sorafenib; Sor-NR, sorafenib non-responder; Sor-R, sorafenib responder; SPP1, secreted phosphoprotein 1; SPP1-APT, SPP1-aptamer; SPP1-BP, SPP1-blocking peptide; sSPP1, secretory SPP1; STAT3, signal transducer and activator of transcription 3; T, tumor; TAMs, Tumor-associated macrophages; TCGA LIHC, The Cancer Genome Atlas liver hepatocellular carcinoma project; TECs, thymic epithelial cells; TKIs, tyrosine kinase inhibitors; TM1, tissue monocytes; TME, tumor microenvironment; TNFSF13, tumor necrosis factor ligand superfamily member 13; TPM, transcripts per million; UMAP, Uniform manifold approximation and projection; UMI, unique molecular identifier; vSMC, vascular smooth muscle cell; WTS, whole-transcriptome sequencing.

JungWoo Eun Jung Hwan Yoon Hye Ri Ahn contributed equally to this work.

Correspondence
Hyo Jung Cho, MD, PhD; Department of Gastroenterology, Ajou University School of Medicine, 164 Worldcup-ro, Yeongtong-gu, Suwon 16499, South Korea.
E-mail: pilgrim8107@hanmail.net

Jae Youn Cheong, M.D, PhD; Department of Gastroenterology, Ajou University School of Medicine, 164 Worldcup-ro, Yeongtong-gu, Suwon 16499, South Korea.
E–mail: jaeyoun620@gmail.com

Funding information
Ministry of Health and Welfare, Republic of Korea, Grant/Award Numbers: HR21C1003, HR22C1734; Bio and Medical Technology Development Program of the National Research Foundation funded by the Korean government, Ministry of Science and Information & Communications Technology, Grant/Award Numbers: NRF-2021R1C1C1009619, NRF-2022R1A2C2092422

Abstract

Background: Cancer-associated fibroblasts (CAFs) play an important role in the induction of chemo-resistance. This study aimed to clarify the mechanism underlying CAF-mediated resistance to two tyrosine kinase inhibitors (TKIs), sorafenib and lenvatinib, and to identify a novel therapeutic target for overcoming TKI resistance in hepatocellular carcinoma (HCC).

Methods: We performed a systematic integrative analysis of publicly available gene expression datasets and whole-transcriptome sequencing data from 9 pairs of CAFs and para-cancer fibroblasts isolated from human HCC and para-tumor tissues, respectively, to identify key molecules that might induce resistance to TKIs. We then performed in vitro and in vivo experiments to validate selected targets and related mechanisms. The associations of plasma secreted phosphoprotein 1 (SPP1) expression levels before sorafenib/lenvatinib treatment with progression-free survival (PFS) and overall survival (OS) of 54 patients with advanced HCC were evaluated using Kaplan-Meier and Cox regression analysis.

Results: Bioinformatic analysis identified CAF-derived SPP1 as a candidate molecule driving TKI resistance. SPP1 inhibitors reversed CAF-induced TKI resistance in vitro and in vivo. CAF-derived SPP1 activated rapidly accelerated fibrosarcoma (RAF)/mitogen-activated protein kinase (MAPK) and phosphatidylinositol 3-kinase (PI3K)/protein kinase B (AKT)/mammalian target of rapamycin (mTOR) through the integrin-protein kinase C-alpha (PKCα) signaling pathway and promoted epithelial-to-mesenchymal transition (EMT). A high plasma SPP1 level before TKI treatment was identified as an independent predictor of poor PFS ($P = 0.026$) and OS ($P = 0.047$) in patients with advanced HCC after TKI treatment.

Conclusions: CAF-derived SPP1 enhances TKI resistance in HCC via bypass activation of oncogenic signals and EMT promotion. Its inhibition represents a promising therapeutic strategy against TKI resistance in HCC. Moreover, plasma SPP1 level before TKI treatment represents a potential biomarker for treatment response prediction.

KEYWORDS
drug resistance, epithelial-to-mesenchymal transition, hepatocellular carcinoma, secreted phosphoprotein 1

1 | BACKGROUND

Hepatocellular carcinoma (HCC) is the fourth leading cause of cancer-related deaths worldwide [1]. HCC with extrahepatic metastasis (M1 or N1) or locally advanced HCC with portal vein invasion is considered advanced-stage HCC and is not amenable to locoregional therapy [2]. Patients with advanced HCC are generally treated with systemic therapeutics, such as tyrosine kinase inhibitors (TKIs) and immune checkpoint inhibitors (ICIs) [3, 4].

Sorafenib and lenvatinib are TKIs that suppress HCC progression by inhibiting various receptor tyrosine kinases (RTKs) [5]. They have been approved by the United States Food and Drug Administration as first-line systemic therapy agents for advanced HCC. Although the treatment paradigm for advanced HCC is shifting toward ICI-based treatments, it is expected that TKIs will remain the first-line treatment in combination with ICIs and a form of rescue therapy after ICI treatment failure [6]. However, since the majority of patients with advanced HCC develop

innate or acquired resistance to TKIs, only 10%–30% of patients exhibit an objective response to sorafenib or lenvatinib [7, 8]. Therefore, the prognosis of patients with advanced HCC remains extremely poor, even after TKI treatment [8, 9]. Therefore, novel therapeutic strategies to overcome TKI resistance in patients with advanced HCC are warranted. Furthermore, biomarkers that predict treatment response are also needed since responses to TKIs vary widely.

Cancer-associated fibroblasts (CAFs) constitute a major stromal cell type within the tumor microenvironment (TME) [10]. Making up the bulk of the tumor stroma, CAFs stimulate tumor cell proliferation, invasiveness, and metastatic potential in various cancer types, including HCC [11, 12]. According to several recent studies, CAFs play a crucial role in the induction of chemo-resistance in different tumors, including HCC [13–15]. However, the mechanism of CAF-mediated TKI resistance in HCC remains to be fully elucidated. This constitutes a crucial step toward the identification of novel therapeutic targets for overcoming chemo-resistance and biomarkers for predicting treatment response.

This study aimed to investigate the mechanism of CAF-induced TKI resistance in HCC to identify novel therapeutic targets for overcoming this resistance. Furthermore, this study sought to identify a promising circulating biomarker for the prediction of treatment response and prognosis before TKI treatment initiation in patients with advanced HCC.

2 | MATERIALS AND METHODS

2.1 | Isolation of fibroblasts from surgically resected liver tissues

The liver tissues and clinical data used in this study were provided by the Biobank of Ajou University Hospital (Suwon, South Korea), a member of the Korea Biobank Network (http://www.kbn.re.kr/kbn/main.do). Cancer and paired para-cancer tissues were collected from patients with HCC who underwent surgical resection as first-line treatment at the Ajou University Hospital between January 2017 and December 2019, with permission from the patients. Patients were included based on the following criteria: (1) age between 18 and 80 years; (2) Barcelona Clinic Liver Cancer (BCLC) stage A; (3) treatment with surgical resection; (4) pathologically confirmed HCC; and (5) consent for the use of surgical specimens for research purposes. Exclusion criteria were as follows: (1) diagnosed with other liver tumor such as cholangiocarcinoma; and (2) no permission from of patients for the use of their surgical specimens for research purposes.

CAFs and para-cancer fibroblasts were isolated from HCC tissues and non-tumor tissues adjacent to the HCC, respectively. Normal fibroblasts (NFs) were isolated and cultured from normal liver tissue acquired from a patient who did not have any chronic liver disease but had undergone surgical resection for hepatic hemangioma, which is known as benign liver tumors.

Fresh liver tissue samples were washed with phosphate-buffered saline (PBS; GenDEPOT, Barker, TX, USA) and finely minced into small pieces (<1 mm^3). Five or six minced small tissues were attached to each well of 6-well plates and cultured. The Dulbecco's modified Eagle's medium (DMEM; GenDEPOT) containing 10% fetal bovine serum (FBS; Invitrogen, Waltham, MA, USA) and 100 units/mL penicillin-streptomycin (GenDEPOT) was changed every two days. Fibroblasts extending from the tissues were trypsinized and transferred to a culture dish, then incubated in a fresh culture medium to promote the attachment of isolated fibroblasts to the culture dish. Cells were maintained in a completed medium, at 37°C in a humidified incubator with 5% CO_2.

2.2 | Immunofluorescence

Isolated fibroblasts were identified via staining for alpha-smooth muscle actin (α-SMA). To avoid CAF senescence, all experiments were performed using fibroblasts up to passage 5. Paraffin-embedded human HCC tissue sections were subjected to hematoxylin and eosin (H&E) staining, and double immunofluorescence (IF) staining was performed with mouse α-SMA (1:100, ab7817, Abcam, Cambridge, UK) and rabbit secreted phosphoprotein 1 (SPP1) primary antibodies (1:100, ab8448, Abcam). Briefly, HCC sections were deparaffinized with xylene, rehydrated, unmasked in sodium citrate buffer (10 mmol/L, pH 6.0), and treated with a glycine solution (2 mg/mL) to quench autofluorescence signals before beginning the immunostaining procedure. After the blockade of non-specific antibody-binding sites by applying a solution of 1% bovine serum albumin in PBS for 1 h at room temperature, tissue slides were incubated overnight at 4°C with a mixture of mouse and rabbit primary antibodies diluted in blocking solution. The following day, the immunoreactions were revealed using fluorescent-dye conjugated secondary antibodies (Invitrogen; Cell Signaling, Danvers, MA, USA) diluted at 1:500 in the blocking solution. After nuclear counterstaining with 4′,6-diamidino-2-phenylindole (DAPI), the immunolabeled slides were examined with an EVOS M5000 microscope (Invitrogen).

Cells were fixed in 3% paraformaldehyde for 20 min at room temperature and permeabilized in 0.5% Triton

X-100 on ice for 7 min. The cells were washed in PBS plus 0.5% normal goat serum and incubated with one of the following primary antibodies: α-SMA (1:100, ab7817, Abcam), SPP1 (1:100, ab8448, Abcam), or integrin subunit β1 (ITGB1, 1:100, ab30394, Abcam). AlexaFluor-488- or AlexaFluor-555-conjugated secondary antibodies were used as required. Nuclear DNA was stained with DAPI. Cells were analyzed using a fluorescent microscope (Zeiss, Oberkochen, Germany) to visualize the endogenous level of proteins under study. Information on the primary and secondary antibodies is presented in Supplementary Tables S1-S2.

2.3 | Collection of cell culture medium

CAFs, para-cancer fibroblasts, and NFs were seeded on 100 mm plates at 5×10^6 cells. Culture medium was removed 24 h after cell seeding, cells were washed once with PBS, and 10 mL of serum-free DMEM (culture medium; CM) including 100 units/mL penicillin-streptomycin was added per plate. After 24 h of incubation at 37°C, the CM was collected and passed through a 0.2 μm membrane syringe filter to remove any cells and cell debris. The CM was stored at -80°C until further use. To examine the effects of CAF-, para-cancer fibroblast-, and NF-derived CM, HCC cell lines Hep3B and Huh-7 were treated with CM (10×).

2.4 | Western blotting

Cells were treated with 10× CAF-CM or 100 ng/mL recombinant SPP1 (rSPP1) to determine whether the signaling mechanism regulated by CAF-CM is due to the SPP1 protein present in CAF-CM. We examined the expression of phosphatidylinositol-3-kinase (PI3K)/protein kinase B (AKT) pathway-related proteins, including PI3K, AKT, and mammalian target of rapamycin (mTOR), and RAS/rapidly accelerated fibrosarcoma (RAF)/mitogen-activated protein kinase (MAPK) pathway-related proteins, including RAS, v-raf murine sarcoma viral oncogene homolog B (BRAF), phosphorylated protein kinase C alpha (PKCα), extracellular signal-regulated kinase (ERK)1/2, and signal transducer and activator of transcription 3 (STAT3). We also analyzed the expression of apoptosis-related proteins, poly(ADP-ribose) polymerase (PARP) and caspase-3, and epithelial-mesenchymal transition-related proteins, including integrin subunit αV (ITGAV), neurotrimin (NTM), cartilage oligomeric matrix protein (COMP), fibroblast activation protein alpha (FAP), E-cadherin, Vimentin, and Snail. α-SMA was confirmed in the isolated NFs, para-cancer fibroblasts, and CAFs. Briefly, cells were lysed in lysis buffer composed of 150 mmol/L NaCl, 25 mmol/L Tris-HCl at pH 8.0, 1% NP-40, 10 mmol/L NaF, 1 mmol/L Na3VO4 and containing protease and phosphatase inhibitor cocktail (Roche, Indianapolis, IN, USA). After determining the protein concentration by Pierce BCA protein assay kit (Thermo Fisher Scientific, Waltham, MA, USA), 20 μg of protein lysates from each sample was resolved in SDS-PAGE and thereafter transferred onto polyvinylidene difluoride membrane. Blots were subjected to blocking for 1 h at room temperature and probed overnight at 4°C with specific primary antibodies followed by appropriate HRP-linked secondary antibodies (Cell Signaling). After brief incubation of membranes with enhanced chemiluminescence (ECL) solution, protein bands were visualized by LAS-4000 Imaging System (Fujifilm, Tokyo, Japan). The membrane band optical density was quantified using the ImageJ software (Laboratory for Optical and Computational Instrumentation, Madison, WI, USA). Information regarding the primary and secondary antibodies is presented in Supplementary Tables S1-S2.

2.5 | Acquisition and analysis of the gene expression profiles in public omics databases

The Cancer Cell Line Encyclopedia (CCLE) database (https://sites.broadinstitute.org/ccle/) was used to analyze the expression of SPP1 mRNA in HCC cells. To analyze gene expression in human and mouse HCC tissues with different sorafenib responses, we obtained microarray data from Gene Expression Omnibus (GEO) database (https://www.ncbi.nlm.nih.gov/geo/) with the accession number GSE109211 and GSE143233. Moreover, to estimate the associations between *SPP1* expression and different clinicopathologic parameters, we used The Cancer Genome Atlas liver hepatocellular carcinoma project (TCGA LIHC) dataset and GSE89377 (Catholic University of Korea's liver hepatocellular carcinoma project, Catholic LIHC).

2.6 | Cell culture and transfection

Human hepatocellular carcinoma cell lines Hep3B, Huh-7, PLC/PRF/5, SNU449, SNU368, and SNU475 cells (detailed information on cell lines can be found at https://cellbank.snu.ac.kr/main/index.html) were certified through the short tandem repeat genotyping and were acquired in March 2021 from the Korean Cell Line Bank (Seoul, South Korea) and cultured in DMEM

or RPMI-1640 containing 10% FBS and 100 units/mL penicillin-streptomycin. The HCC cell line used in all in vivo assays was Huh-7. Cells were transiently transfected with small interfering RNA (siRNAs) against ITGB1 (s7575, Thermo Scientific, Waltham, MA, USA), ITGB5 (s7590, Thermo Scientific), or negative control (4457287, Thermo Scientific) using Lipofectamine3000 transfection reagent (Invitrogen), according to the manufacturer's instructions.

2.7 | RNA extraction and quantitative reverse transcription-polymerase chain reaction (qRT-PCR)

Total RNA was isolated from HCC cell lines using TRIzol reagent (Invitrogen). cDNA was synthesized from 500 ng of total RNA using 5X PrimeScript™ RT Master Mix (Takara Bio, Shiga, Japan). qRT-PCR was performed using amfiSure qGreen Q-PCR Master Mix (GenDEPOT) and monitored in real-time using a CFX Connect Real-Time PCR Detection System (Bio-Rad Laboratories, Hercules, CA, USA). The cycling conditions were as follows: 95°C for 2 min, 40 cycles of 95°C for 15 s, 56—58°C for 34 s, and 72°C for 30 s, followed by a dissociation stage at 95°C for 10 s, 65°C for 5 s, and 95°C for 5 s. Relative gene expression levels were calculated using the $2^{-\Delta\Delta Ct}$ method, and glyceraldehyde 3-phosphate dehydrogenase (*GAPDH*) was used for normalization. The primer sequences were used as follows: SPP1: forward, 5′-CTTCTCAGCCAAACGCCGAC-3′; reverse, 5′-ACACAGCATTCTGCTTTTCCTCA-3′. GAPDH: forward, 5′-AGTATGACAACAGCCTCAAG-3′; reverse, 5′-TCATGAGTCCTTCCA CGATA-3′. All measurements were performed in triplicate.

2.8 | Measurement of cell viability and proliferation

Hep3B and Huh-7 cells were treated with 10× NF-CM, 10× para-cancer fibroblast-CM, or 10× CAF-CM in combination with 15 μmol/L sorafenib or 5 μmol/L lenvatinib in a 24-well plate at a density of 7×10^4 cells/well and incubated at 37°C for 24 h. Next, 50 μL of 3-(4,5-dimethylthiazol-2-yl)-2,5-diphenyltetrazolium bromide (MTT; 1 mg/mL, Merck KGaA, Darmstadt, Germany) was added to each well of the plate and incubated for 1 h at 37°C in the dark. The supernatant was carefully aspirated, and 500 μL of dimethyl sulfoxide (DMSO; Ducksan, Gwangju, South Korea) was added, following which optical density values at 570 nm were measured using a Promega Glomax microplate reader (Promega, Madison, Wisconsin, USA).

To analyze cell proliferation, 5-bromo-2′-deoxyuridine-5′-monophosphate (BrdU) incorporation was determined by estimating the DNA uptake of BrdU. Cells were plated into 24-well plates at 5×10^4 cells per well for 24 h and measured using a BrdU enzyme-linked immunosorbent assay (ELISA) kit (11647229001, Roche) according to the manufacturer's instructions.

2.9 | Caspase 3/7 activity assays

Apoptosis activation of cells cultured in NF-CM, para-cancer fibroblast-CM, or CAF-CM in combination with 15 μmol/L sorafenib or 5 μmol/L lenvatinib was evaluated using Caspase-Glo 3/7 (G8090, Promega) and Cell-titer-Glo assays (G7570, Promega), according to the manufacturer's instructions. Each sample was analyzed in triplicate.

2.10 | SPP1-blocking peptide and SPP1-aptamer

SPP1-blocking peptide (SPP1-BP) was purchased from PromoCell (pk-ab718-7443p, Heidelberg, Germany), and SPP1-aptamer (SPP1-APT) was custom-synthesized by Bioneer (Daejeon, South Korea). The sequence of SPP1-APT was 5'-CGGCCACAGAAUGAAAAACCUCAUCGAU GUUGCAUAGUUG-3'. The aptamer was modified at the 2′-O position with a methyl group and included phosphorothioate-modified bases to help protect the nucleic acids from rapid attack by endo- and exonucleases.

2.11 | Establishment of sorafenib- and lenvatinib-resistant cells

To determine the half maximal inhibitory concentration (IC_{50}) of HCC cells to sorafenib (SMB2653, Sigma, Burlington, MA, USA) and lenvatinib (SML3017, Sigma), HCC cells were incubated with different concentrations of sorafenib and lenvatinib in 96-well plates, and cell viability was measured three days later as described below. The cells were cultured in 6-well plates at 1×10^4 cells/well and incubated with sorafenib and lenvatinib at a concentration just below their respective IC_{50} values. The concentrations of sorafenib and lenvatinib were slowly increased by 0.5 μmol/L per week. After five weeks, two sorafenib- and lenvatinib-resistant cell lines were obtained, termed Hep3B-resistance cells (Hep3B-R) and Huh-7-resistance cells (Huh-7-R), respectively, and were continuously maintained by culturing them in the presence of sorafenib and lenvatinib.

2.12 | Mouse tumor models

We designed three different in vivo experiments (Supplementary Table S3).

For subcutaneous xenograft models (in vivo 1 and in vivo 2), 5-week-old female BALB/c nude mice, purchased from ORIENT BIO (Seongnam, South Korea), were bred in an individually ventilated cage system under pathogen-free conditions with food and water ad libitium and regular 12 h light/12 h dark and allowed to acclimatize for one week before experiments. In the in vivo 1 assay, mice were divided into two groups, each consisting of five mice. All injections were administered into the right flank of the nude mice. The first group was injected with Huh-7 cells and treated with sorafenib (Sor). The second group was co-injected with Huh-7 cells and CAFs followed by sorafenib treatment (CAF + Sor). In the in vivo 2 assay, mice were randomly divided into four groups, each consisting of five mice. All injections were administered into the right flank of the nude mice. The first group was co-injected with Huh-7 cells and CAFs, and observed without any treatment (CAF). The second group was co-injected with Huh-7 cells and CAFs followed by sorafenib treatment (CAF + Sor). The third group was co-injected with Huh-7 cells and CAFs followed by sorafenib and SPP1-APT combination treatment (CAF + Sor + SPP1-APT). The fourth group was injected with Huh-7 cells without CAFs and treated with sorafenib (Sor). We generated mouse xenograft tumors by subcutaneously injecting 5×10^5 Huh-7 into the left flank of each mouse, either alone or mixed with 2.5×10^5 CAFs. When tumor volumes reached 100 mm^3, treatment was initiated and administered according to the protocol. Sorafenib (10 mg/kg/day; Sigma) was administered orally, and SPP1-APT (2 mg/kg/day; Bioneer) was injected into the intraperitoneal cavity. The tumor diameter and body weight were measured every two days using a digital caliper and digital scale, respectively. Tumor volume was calculated as per the following formula: Tumor volume (mm^3) = 0.52 × length × $width^2$. Three weeks after cell injection, the mice were euthanized by CO_2 inhalation, and the tumors were removed for weighing and histological analysis. All the animals were cared in keeping with the Guide for the Care and Use of Laboratory Animals, and experiments were approved by the Ethics Committee for Laboratory Animal Research Center of Ajou University Medical Center (IACUC-2020-0038, Suwon, South Korea). Humane endpoints were set as follows: 20% body weight loss, loss of mobility, and activity. However, no mice reached these humane endpoints during the study.

Tumor tissue samples were fixed with 10% neutral buffered formalin for H&E and immunohistochemistry (IHC) staining. The sections were incubated with the human-specific primary antibodies against SPP1 (1:200, AF1433, R&D systems, Minneapolis, MN, USA), Ki67 (1:500, ab15580, Abcam), E-cadherin (1:100, 610404, BD Biosciences, Franklin Lakes, New Jersey, USA), α-SMA (1:200, ab7817, Abcam) and Fibronectin (1:100, sc8422, Santa Cruz Biotechnology, Dallas, TX, USA). ImageJ software was used to measure and quantify the intensity of the stained area.

In the orthotopic xenograft model (in vivo 3), we anesthetized the mice with an intraperitoneal injection of a ketamine/rompun solution (50 mg/kg ketamine and 5 mg/kg rompun). We then generated mouse tumors by injection of 5×10^5 Huh-7 cells either alone or mixed with 2.5×10^5 CAFs. The cells were mixed with Matrigel (354230, Corning, New York, USA) and kept in ice until the moment of the injection. A 1.5 cm skin incision was made in the upper abdominal wall, followed by a 1 cm incision in the peritoneum to expose the liver. Injection was performed into the left liver lobes of each mouse, and the change of color of the liver was observed during the injection. After injection, the incision and the skin were closed. One week after cell injection, treatment was initiated according to the treatment conditions (Supplementary Table S3). On day 12, we opened the skin and checked for tumor development. Three weeks after cell injection, the mice were euthanized, and livers were removed for liver and tumor weights at the end of the experiment.

2.13 | RNA-sequencing data analysis

To investigate major CAF-derived molecules that induce TKI resistance in HCC, we analyzed whole-transcriptome sequencing (WTS) data of 9 pairs of CAF and para-cancer fibroblast samples and one NF sample from surgically resected human liver tissues (Supplementary Figure S1A). For next-generation RNA-sequencing (RNA-seq) analysis, total RNA was extracted from NFs, para-cancer fibroblasts, and CAFs using the TRIzol reagent. RNA quality control was performed with the Agilent Bioanalyzer system (Agilent Technologies, Santa Clara, CA, USA). The sequencing library was prepared with Truseq Stranded Total RNA Sample Preparation Kit (Illumina, San Diego, CA, USA), followed by library quality check using the Agilent Bioanalyzer system. Sequencing was performed on Illumina HiSeq2000 machines (Illumina) using the standard Illumina RNAseq protocol with a read length of 200 bases. All sequenced reads were quality checked using FastQC followed by mapping to the human reference genome GRCh38 and the Ensembl release-102 version 73 gene annotation using HISAT2 (v2.2.1). To compare expression between genes within samples, gene expression was estimated using StringTie v2.1.4 from the

"new Tuxedo" package. Gene abundances were normalized to library and gene length by calculating fragments per kilobase of exon per million mapped reads using featureCounts, and differentially expressed genes were identified by count data with DESeq2. The raw data had been uploaded to the GEO database (Accession Number: GSE192912) of the National Center for Biotechnology Information (NCBI).

2.14 | Molecular pathway mining and network analysis

To investigate molecular pathways of gene signatures, we uploaded 790 CAF-specific gene signatures or 1,601 SPP1-related gene signatures to the Molecular Signatures Database (MSigDB, http://software.broadinstitute.org/gsea/msigdb) via the Broad Institute Gene Set Enrichment Analysis (GSEA; http://www.broadinstitute.org/gsea). GSEA was conducted by computing overlaps with the canonical pathway (C2). Genes in Gene Set (K), Genes in Overlap (k), k/K ratio and *P* value were used to rank the pathways enriched in each phenotype.

The protein-protein network was established via the GPS-Prot interaction network (http://gpsprot.org), and module analysis was performed using Cytoscape 3.7.0 (http://www.cytoscape.org/, Institute for Systems Biology, Seattle, DC, USA). The hub genes of SPP1 were selected for further bioinformatics analysis using the gene multiple association network integration algorithm (GeneMANIA) App of Cytoscape, which contains a comprehensive set of datasets from the Biological General Repository for Interaction Datasets (BioGRID), Pathway Commons, and GEO, as well as organism-specific functional genomics datasets. The biological process of SPP1 hub genes was also visualized using the Biological Networks Gene Oncology (BiNGO) tool (version 3.0.3) plugin of Cytoscape.

2.15 | Immunohistochemical assessment of SPP1 expression in human HCC tissues

IHC was performed to evaluate SPP1 expression relative to the location of CAFs and tumor cells within HCC tissues. IHC staining was performed on 4-μm-thick, FFPE tissue sections using an automated immunostainer (Ventana Medical Systems, Oro Valley, AZ, USA) according to the manufacturer's protocol. The anti-SPP1 (Osteopontin) antibody (ab8448, Abcam) was utilized at 1:300 dilution to stain the tissue samples. The staining intensity of cancer cells and fibroblasts was scored as follows: 0, no reactivity or faint staining; 1+, faint or weak staining; 2+, moderate staining; 3+, strong staining. To assess the degree of SPP1 staining, the H-score was calculated as per the following equation: H-score = 3 × (% of 3+ staining area) + 2 × (% of 2+ staining area) + 1 × (% of 1+ staining area).

Two board-certificated pathologists (SK and YBK) with gastrointestinal pathology specialty independently interpreted the IHC slides. The pathologists initially made a consensus of 0/1+/2+/3+ cells of SPP1 expression with a control sample of breast cancer, which was recommended by the manufacturer of the antibody. Following the independent reading of the HCC tissue sections, any case showing a discrepant H-score was reviewed and a consensus was arrived at by the pathologists. The participating pathologists were blinded to the clinical data of the patients.

2.16 | Fluorescence quantitative analysis for protein expression of integrins

The fluorescence intensity of integrins and β-actin in Hep3B and Huh-7 cells were measured with fluorescence microplate reader (Glomax discovery, Promega). We seeded 2×10^3 cells in a 96-well black plate and performed IF staining using each integrin and beta-actin antibody. For IF staining, cells were fixed with 4% paraformaldehyde in PBS, and cell membrane was permeabilized using 0.5% Triton X-100. These samples were blocked with 3% bovine serum albumin blocking solution at room temperature and then incubated with primary antibody, followed by incubation with fluorescence-conjugated secondary antibody (Invitrogen). Finally, the fluorescence intensity was measured (integrins, λex = 475 nm, λem = 500-550 nm; β-actin, λex = 627 nm, λem = 660-720 nm) using a Glomax discover microplate reader. To calculate the expression of integrins, the measured integrin fluorescence intensity was divided by the β-actin fluorescence intensity. Information regarding primary and secondary antibodies is provided (Supplementary Tables S1-S2).

2.17 | Wound healing assay

When Huh-7 cell density reached 100%, wounds were created in the central area using a 200 μL pipette tip. Photos of the scrape line were taken at 0 and 24 h. Each experiment was repeated thrice. Cell migration was expressed as the percentage of wound closure in the wound area. Image analysis was performed via ImageJ software.

2.18 | Transwell assay

Transwell chambers (Corning) without Matrigel were used to examine cell migration, and transwell chambers coated

with 50 μL Matrigel (354234, Corning) were used to measure invasion; 5×10^4 cells were serum-starved for 12 h, resuspended in 100 μL serum-free medium and added to the upper compartment of the chamber, while the bottom chamber was filled with medium supplemented with 10% FBS. After incubation at 37°C in a 5% CO_2 humidified atmosphere for 24 h, the chambers were analyzed for migration and invasion. The experiments were independently repeated thrice.

2.19 | Co-immunoprecipitation (co-IP)

To identify receptors that bind to SPP1 on HCC cells, Hep3B and Huh-7 cells were transfected with *siITGB1* and/or *siITGB5*, or siCtrl. Then, they were cultured with CAF-CM, and co-IP experiments were performed. Briefly, cells were washed with PBS and lysed at 4°C with PBS, pH 7.2, containing 1.0% NP-40, 0.5% sodium deoxycholate, 0.1% SDS, 10 mmol/L NaF, 1.0 mmol/L $NaVO_4$, and a 1.0% protease inhibitor cocktail (Sigma) as previously described [16]. Equal protein aliquots (1.0 mg) were immunoprecipitated with 2.0 μg of antibodies specific to SPP1 (STJ25679, St. John's laboratory, London, UK) plus protein A/G-agarose (sc-2003, Santa Cruz Biotechnology, Santa Cruz, CA, USA) as per the manufacturer's recommendations. Immunoprecipitated proteins were resolved on 10% SDS-polyacrylamide gels and transferred to polyvinylidene fluoride membranes (Bio-Rad, Richmond, CA, USA). The membranes were blocked for 1 h in PBS containing 0.1% Tween 20 (PBS-T) and 5% non-fat dry milk (Sigma) and reacted with antibodies against SPP1, ITGB1, ITGB5 (3629, Cell Signaling), integrin subunit α5 (ITGA5; 4705, Cell Signaling), and ITGAV (4711, Cell Signaling), each diluted to 1:1,000. The membranes were washed with PBS-T, and incubated for 1 h at room temperature with horseradish peroxidase-conjugated anti-mouse (A9044, Sigma) or anti-rabbit immunoglobulin G (IgG) antibody (AP160P, Sigma), diluted to 1:5,000, and developed with luminol-based enhanced chemiluminescence plus Western blotting detection system (Amersham Biosciences, Amersham, Buckinghamshire, UK). Immunoreactive bands were identified by co-migration of prestained protein size markers (Fermentas, Glen Burnie, MD, USA). Information regarding primary and secondary antibodies is presented in Supplementary Tables S1-S2.

2.20 | Single-cell RNA-seq analysis

Unique molecular identifier (UMI) counts and metadata of filtered cells from patients with HCC, liver metastases, or cholangiocarcinomas were obtained from the NCBI GEO database under accession codes GSE151530 and GSE146409. The R Seurat package (v4.0.1) was used to perform log normalization, feature selection (method = 'vst'), scaling of data, principal component analysis (PCA), cell clustering, non-linear dimensional reduction (e.g., *UMAP* plotting), and heatmap generation. Briefly, the most variable genes (n = 3,000) across the filtered cells were selected to perform PCA on the scaled data using the FindVariableFeatures function. The FindNeighbors and FindClusters functions were used to construct a shared nearest neighbor (SNN) graph ('dims = 1:30') and cluster the cells ('resolution = 1'), respectively. The RunUMAP function was used with 50 PCA dimensions ('dims = 1:50') to visualize cells on the 2-D UMAP plot. Previously defined cell types [17] were used to classify cells in the generated UMAP plot. Cells annotated as 'CAFs' were extracted and used to generate an independent Seurat object, wherein the same parameters were applied for the abovementioned functions except for the RunUMAP function, which used 30 PCA dimensions ('dims = 1:30'). The Seurat object was used to identify distinct subpopulations of fibroblasts and differential expression features using the FindAllMarkers function. GSEA of the enriched genes was performed using the 'MSigDB Hallmark' database.

2.21 | Patients and definition of clinical terms

To investigate whether the plasma levels of the selected CAF-derived molecule could be used as a biomarker for predicting the response to sorafenib/lenvatinib in patients with advanced HCC, patients were retrospectively included based on the following criteria: (1) age between 18 and 80 years; (2) BCLC stage C; (3) treatment with sorafenib or lenvatinib for a period longer than 4 weeks; (4) availability of follow-up computed tomography (CT) or magnetic resonance (MR) imaging for the assessment of drug response; and (5) stored available plasma acquired within 1 month prior to sorafenib/lenvatinib treatment. Exclusion criteria were as follows: (1) previous history of a primary malignancy other than HCC; (2) Eastern Cooperative Oncology Group (ECOG) performance status 3 or 4; and (3) Child-Pugh class C. HCC was diagnosed based on the European Association for the Study of the Liver guideline [2] and the American Association for the Study of Liver Diseases practice guidelines [18]. Stipulations of the BCLC staging system and modified Union for the International Cancer Control (mUICC) staging system were used for HCC staging [19]. Sorafenib-treated patients received 400 mg of sorafenib twice daily, and lenvatinib-treated

patients received 8 mg (body weight < 60 kg) or 12 mg (body weight ≥ 60 kg) of lenvatinib once daily. Treatment was continued until disease progression or the development of unacceptable drug-related adverse events (AEs). Once AEs occurred, TKI doses were modified depending on the type and grade of AEs [20]. Medical data, including sex, age, Child-Pugh class, tumor number, tumor size, HCC stage, duration of the treatment, progression-free survival (PFS), disease-free survival (DFS), and overall survival (OS), were recorded. Tumor response was assessed according to the modified Response Evaluation Criteria in Solid Tumors (RECIST) criteria 1.1 [21]. PFS was defined as the time from sorafenib/lenvatinib treatment initiation to disease progression. OS was defined as the time from treatment initiation to death from any cause. Baseline laboratory data, including platelet count, total bilirubin, serum creatinine, albumin, alanine transaminase, prothrombin time, and alpha-fetoprotein (AFP) were collected. Plasma SPP1 levels were measured using ELISA. Serum samples and clinical data were provided by the Biobank of Ajou University Hospital, a member of the Korea Biobank Network.

2.22 | Statistical analyses

OS, DFS and PFS curves were plotted via the Kaplan-Meier product limit method using GraphPad™ 8.0 software (GraphPad Software, San Diego, CA, USA). Significant differences between survival curves were determined using the log-rank test and Breslow test. Receiver-operating characteristic curve was used to determine the best cut-off values for SPP1 that could produce the highest sensitivity and specificity to predict individual survival shorter than the median PFS or OS. We performed Cox regression analysis to determine variables associated with prognosis. Multivariate Cox regression analyses were performed with clinical variables known to be of prognostic value in TKI-treated patients to identify independent risk factors for predicting poor PFS and OS. Model 1 was derived by backward elimination selection procedure after entering all of the listed clinical variables into the multivariate analysis. Model 2 was derived from all of the listed clinical variables without any variable selection procedure. All experiments were performed at least in triplicate. All samples were analyzed in triplicate. All data are presented as the mean ± standard error of the mean (SEM). Significant differences between experimental groups were assessed using paired or unpaired Welch's *t*-tests and one- or two-way analysis of variance (ANOVA) in GraphPad™ 8.0 software. Statistical significance was set at $P < 0.05$.

3 | RESULTS

3.1 | CAFs suppressed the sensitivity of HCC cells to sorafenib and lenvatinib

CAFs, para-cancer fibroblasts, and NFs exhibited spindle-shaped morphology (Supplementary Figure S1B). α-SMA was overexpressed in CAFs relative to para-cancer fibroblasts and NFs (Figure 1A and Supplementary Figure S1C). The paracrine effect of CAFs on HCC concerning sorafenib and lenvatinib sensitivity was evaluated. On cell viability, cell proliferation, and caspase 3/7 activity assays, TKI response was shown to be significantly lower in HCC cells incubated with CAF-CM than in HCC cells incubated with para-cancer fibroblast-CM or NF-CM (Figure 1B-D).

Next, Western blotting (Supplementary Figure S1D) and corresponding densitometry analyses (Supplementary Figure S1E) revealed that CAF-CM exerted a protective effect on HCC cells against TKI-induced apoptosis. These results indicate that CAF induced TKI resistance in a paracrine manner. Furthermore, in the in vivo 1 assay, the CAF + Sor group exhibited significantly higher tumor volumes than the Sor group ($P < 0.001$; Figure 1E).

3.2 | Identified genes specifically overexpressed in CAFs

In the cluster analysis, 790 genes were significantly overexpressed in CAFs compared to para-cancer fibroblasts and NFs (Figure 2A). GSEA indicated that genes specifically overexpressed in CAFs were enriched in various cancer-associated pathways, including the EMT and Kirsten rat sarcoma virus (KRAS) signaling pathways (Figure 2B). Of the 790 genes overexpressed in CAFs, 245 genes which were overexpressed greater than 1.5-fold change ($P < 0.001$) in CAFs relative to para-cancer fibroblasts or NFs were selected for next step (Figure 2C). Then, we selected only secretory protein-encoding genes among the 245 genes for further analyses given that CAF induced TKI resistance mainly in a paracrine manner (Figure 1). As a result, 9 secretory protein-encoding genes were selected as candidate molecules for further investigation (Figure 2C).

3.3 | SPP1 was overexpressed in HCC tissues from sorafenib non-responders

Expression levels of the 9 candidate genes were evaluated in HCC tissue expression data from the GSE109211 dataset (STORM phase III study [22]; Figure 2D). GSE109211 includes gene expression data of HCC tissues and clinical

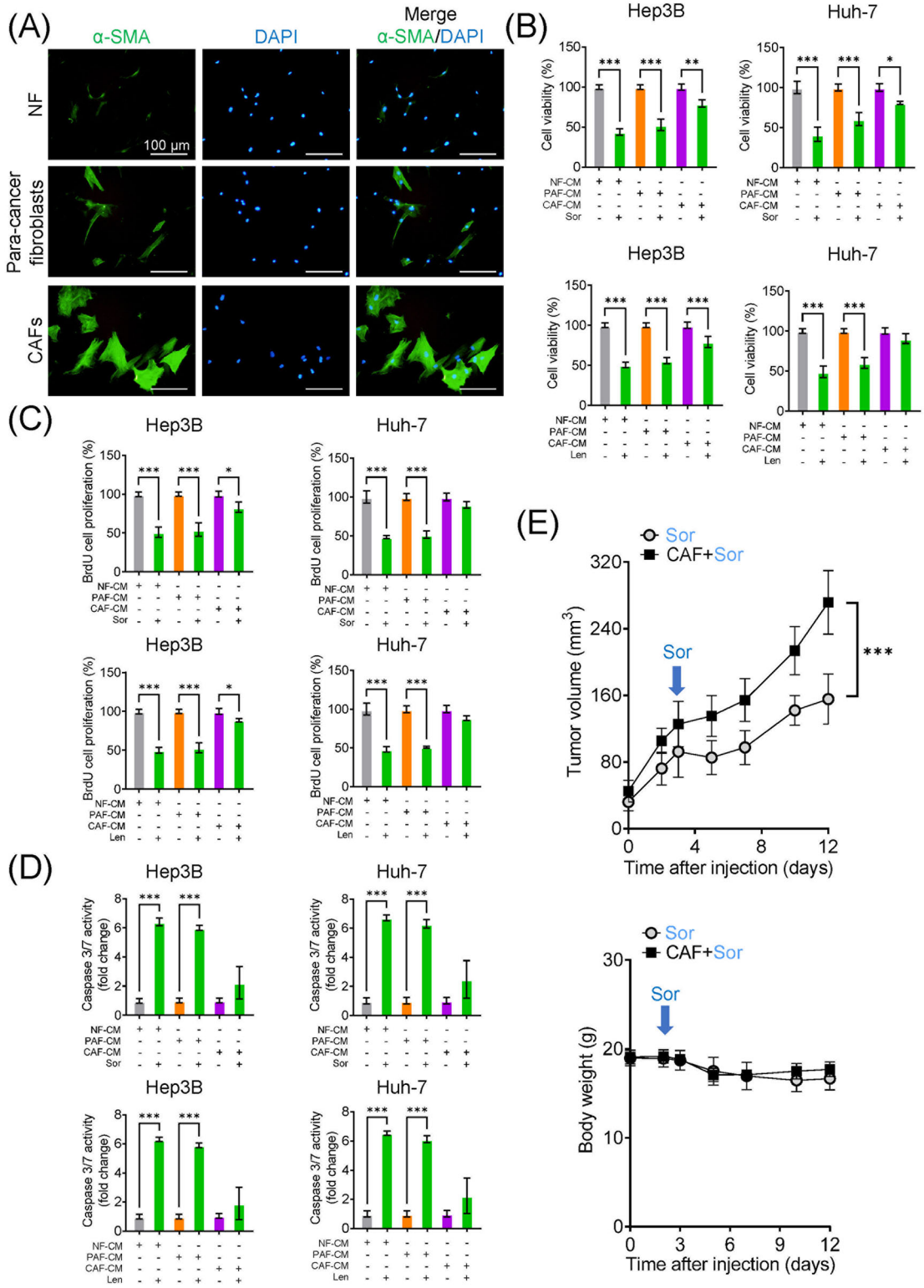

FIGURE 1 CAFs suppressed the sensitivity of HCC cells to sorafenib and lenvatinib. (A) Immunofluorescence analysis for the levels of α-SMA in isolated fibroblasts. (B-D) CAF-CM-incubated HCC cells (Hep3B and Huh-7 cells) showed significantly lower sensitivity to sorafenib (15 μmol/L) or lenvatinib (5 μmol/L) compared to para-cancer fibroblast-CM- or NF-CM-incubated HCC cells based on cell viability (B), cell proliferation (C), and caspase 3/7 activity assays (D). (E) Comparison of changes in mean tumor volume (top) and body weight (bottom) during sorafenib treatment between the groups. (mean ± SEM; One-way ANOVA test; $^{*}P < 0.05$; $^{**}P < 0.01$; $^{***}P < 0.001$). Abbreviations: α-SMA, alpha smooth muscle actin; DAPI, 4′, 6-diamidino-2-phenylindole; NF, normal fibroblast; CAFs, cancer-associated fibroblasts; PAF, para-cancer fibroblast; CM, culture medium; Sor, sorafenib; Len, lenvatinib; BrdU, 5-bromo-2'-deoxyuridine-5'-monophosphate.

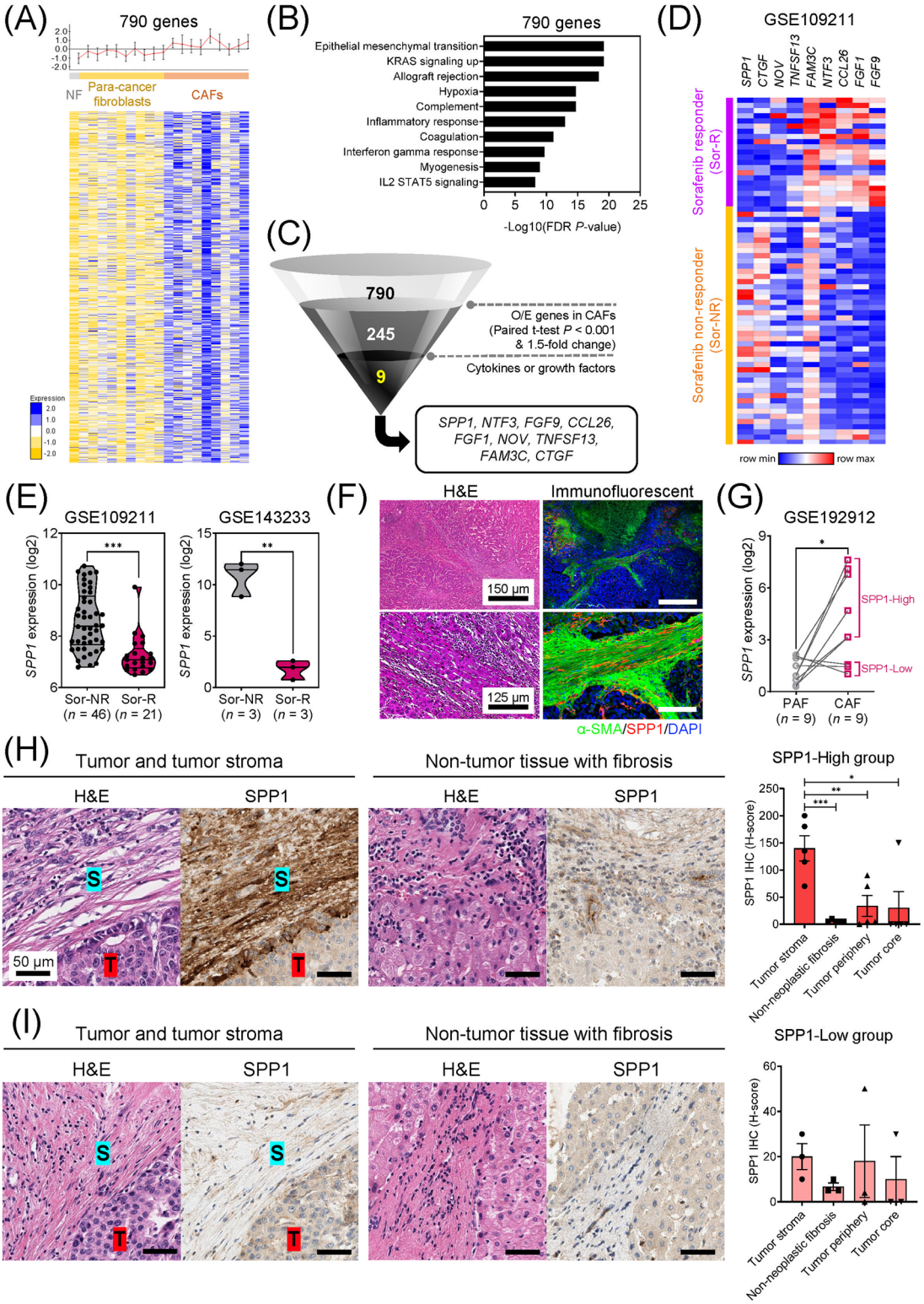

FIGURE 2 Identification of the CAF-derived molecules that induce resistance to sorafenib or lenvatinib in patients with HCC. (A) Heat map of 790 genes overexpressed in CAFs. (B) GSEA of the genes overexpressed in CAFs. (C) Process of candidate gene selection. (D) Expression levels of the 9 candidate genes according to sorafenib response in the GSE109211 dataset. (E) Comparison of *SPP1* expression between sorafenib responders and non-responders in the GSE109211 and GSE143233 datasets. (F) Immunofluorescence staining of α-SMA and SPP1 in tumor tissues from patients with HCC. (G) Comparison of *SPP1* expression between CAFs and their paired para-cancer fibroblasts in the WTS data from the 9 pairs of CAF and para-cancer fibroblasts. (H) Representative H&E and SPP1 IHC images of the tumor (T), tumor stroma (S) (left), and non-tumor fibrous tissue (middle) in an SPP1-high patient. Scale bar, 50 μm. Comparison of SPP1 IHC staining intensity according to tumor location in the SPP1-high group (right). (I) Representative H&E and SPP1 IHC images of tumor (T), tumor stroma (S)

information on sorafenib response. Among the 9 candidate genes, *SPP1* was identified as significantly overexpressed in sorafenib non-responders compared to responders (Figure 2E, left). The same pattern was observed in another publicly available gene expression dataset (GSE143233; Figure 2E, right).

3.4 | Selection of HCC cell lines for further functional study

Further studies were planned to perform using HCC cells with relatively low *SPP1* expression to investigate the bio-function of CAF-derived SPP1 in HCC cells. The gene expression data of HCC cell lines were downloaded from the CCLE database, and *SPP1* expression in each HCC cell line was evaluated to identify cell lines with low SPP1 expression (Supplementary Figure S2A). Further, we also performed qRT-PCR to evaluate *SPP1* expression in HCC cell lines including Hep3B, Huh-7, PLC/PRF/5, SNU449, SNU368, and SNU475 cells (Supplementary Figure S2B). Hep3B and Huh-7 demonstrated relatively low *SPP1* expression compared to the other cell lines both in CCLE data and qRT-PCR results. Therefore, we performed further functional studies using Hep3B and Huh-7 cells.

3.5 | CAFs were a major source of secretory SPP1 in the HCC TME

To identify the major source of secretory SPP1 within the HCC TME, SPP1 levels were evaluated in cell lysates and CM of two HCC cell lines, CAFs, para-cancer fibroblasts, and NFs via Western blotting and relative densitometry bar graphs (Supplementary Figure S2C). SPP1 expression was the highest in CAF-CM and CAF cell lysates compared to those from other cell lines.

Next, we validated the co-localization of SPP1 and α-SMA in paraffin-embedded HCC tissues using IF staining (Figure 2F). As expected, CAFs in the HCC tumor stroma demonstrated strong α-SMA expression, indicating that CAFs are the major component of the HCC stroma. α-SMA-positive CAFs were observed in the tumor stroma located in not only the tumor periphery but also the center of the tumor bulk. The co-expression of SPP1 in α-SMA-positive CAFs was observed.

Figure 2G shows a comparison of *SPP1* expression between CAFs and para-cancer fibroblasts in WTS data from 9 pairs of CAFs and para-cancer fibroblasts. We categorized 5 patients with *SPP1* overexpression in CAFs relative to their paired para-cancer fibroblasts into the SPP1-high group, and categorized the others into the SPP1-low group. The SPP1-high group exhibited strongly positive staining for SPP1 in the tumor stroma compared to non-tumor fibrous tissue, the tumor core, and the tumor periphery upon IHC analysis. In the comparison of the SPP1 expression between the SPP1-high and SPP1-low groups, SPP1 expression in the tumor stroma was markedly higher in the SPP1-high group compared to the SPP1-low group (Figure 2H-I), and it was consistent with the RNA expression data; as expected, there was no significant difference in the comparison of non-tumor fibrous tissue, tumor core, and tumor periphery between the groups (Supplementary Figure S2D). Taken together, these results confirm that CAFs are the major source of secretory SPP1 within the HCC TME.

Moreover, to evaluate whether *SPP1* expression changes in sorafenib- or lenvatinib-resistant HCC cells, we evaluated *SPP1* expression in Hep3B-R and Huh-7-R cells. Hep3B-R and Huh-7-R cells demonstrated significantly higher IC_{50} than the wild-type Hep3B or Huh-7 cells (Supplementary Figure S2E-F). Subsequently, we evaluated *SPP1* expression in the wild-type HCC cells, sorafenib-/lenvatinib-resistant HCC cells, and CAFs. While there was no significant difference in *SPP1* expression between the resistant cells and the wild-type HCC cells, *SPP1* was specifically overexpressed in HCC-CAFs (Supplementary Figure S2G-H). These results suggest that *SPP1* is mainly expressed in CAFs rather than in resistant HCC cells.

3.6 | Blockade of CAF-derived SPP1 restored HCC cell sensitivity to sorafenib or lenvatinib

IF staining indicated that the uptake of CAF-derived SPP1 in HCC cells was effectively blocked by SPP1 inhibitors, SPP1-BP and SPP1-APT (Supplementary Figure S3A). We subsequently investigated whether SPP1-BP would reverse CAF-induced resistance to sorafenib and lenvatinib in HCC cells. In cell growth, cell proliferation, cell viability, and caspase 3/7 activity assays, CAF-derived SPP1

(left), and non-tumor fibrous tissue (middle) in an SPP1-low patient. Comparison of SPP1 IHC staining intensity according to tumor location in the SPP1-low group (right). (Mean ± SEM; unpaired Welch's *t*-test; $*P < 0.05$; $**P < 0.01$; $***P < 0.001$).

Abbreviations: HCC, hepatocellular carcinoma; NF, normal fibroblast; CAFs, cancer-associated fibroblasts; ELISA, enzyme linked immunosorbent assay; H&E, hematoxylin and eosin; α-SMA, alpha smooth muscle actin; SPP1, secreted phosphoprotein 1; DAPI, 4′, 6-diamidino-2-phenylindole; PAF, para-cancer fibroblast; S, tumor stroma; T, tumor; IHC, immunohistochemistry.

reduced HCC cell sensitivity to sorafenib and lenvatinib (Supplementary Figure S3B). However, the TKI sensitivity of CAF-CM-incubated HCC cells was restored via SPP1-BP treatment. Similar results were observed when Huh-7 cells were treated with rSPP1, with or without SPP1-BP (Supplementary Figure S3C).

Wound-healing, migration, and transwell invasion assays were performed to assess the migratory and invasive potentials of cells. Sorafenib or lenvatinib treatment significantly decreased the capacity of Huh-7 cells for wound healing, migration, and invasion (Figure 3A-C). Interestingly, SPP1-BP treatment restored the decreased sensitivity of CAF-CM- or rSPP1-treated HCC, resulting in a significant decrease in wound-healing, migration, and invasion capacities (Figure 3D-F and Supplementary Figure S4).

3.7 | In vivo validation of the effect of blocking CAF-derived SPP1 on HCC resistance to TKIs

In the subcutaneous xenograft HCC model established using Huh-7 cells (in vivo 2), the CAF group had the highest mean tumor volume and weight; the CAF + Sor group demonstrated significantly larger and heavier tumors than the Sor group; the CAF + Sor + SPP1-APT group showed significantly reduced tumor volume and weight compared to the CAF + Sor group (Figure 4A-C). These results suggest that inhibiting SPP1 could restore CAF-induced sorafenib resistance. We then performed IHC analysis of the isolated tumor tissues, and differences were observed by quantifying the stained area in tumor sections (Figure 4D-E). The levels of α-SMA, Fibronectin, SPP1, and Ki67 expression were significantly lower and the level of E-cadherin expression was higher in the CAF + Sor + SPP1-APT group compared to both the CAF group and the CAF + Sor group. This suggests that the sorafenib and SPP1-APT combination therapy effectively suppresses the proliferation and EMT of tumor cells by inhibiting CAF-derived SPP1 in vivo. This was further confirmed using the orthotopic xenograft HCC model which more accurately represented the HCC TME [23]. Figure 4F shows representative liver and orthotopic tumor images on day 0, day 12, and day 21 after cell injection. The results of the orthotopic xenograft model were quite similar to those of the subcutaneous xenograft model. There was no difference in body weight between the groups in the orthotopic xenograft model (Supplementary Figure S5A). The CAF + Sor + SPP1-APT group demonstrated the smallest tumor volume compared to the other groups (Figure 4G). In the comparison of tumor weight, the CAF + Sor + SPP1-APT group had significantly reduced tumor weight compared to the CAF group (Figure 4H). Furthermore, we compared the number of intrahepatic metastatic foci between the groups (Figure 4I and Supplementary Figure S5B). The CAF group demonstrated a significantly higher number of intrahepatic metastatic foci compared to the other groups. No intrahepatic metastasis was observed in the CAF + Sor + SPP1-APT and Sor groups.

3.8 | CAF-derived SPP1 bound to integrin complexes on the HCC cell surface

We explored SPP1 receptor-binding proteins (RBPs) in HCC cells. As reported in previous studies [24, 25], the protein-protein network analysis revealed CD44 and various integrins as important SPP1 RBPs (Supplementary Figure S6). Among the candidate RBPs, ITGA5, ITGAV, ITGB1, and ITGB5 were expressed in Hep3B and Huh-7 cells, whereas other integrins and CD44 were not (Figure 5A). We subsequently confirmed the similar expression patterns of CD44 and integrins in Hep3B and Huh-7 cells using fluorescence intensity (Figure 5B). co-IP experiments confirmed the binding of SPP1 to ITGA5, ITGAV, ITGB1, and ITGB5 in HCC cells (Figure 5C). Hep3B and Huh-7 cells were transfected with *siITGB1* and/or *siITGB5* to silence ITGB1 and ITGB5, respectively (Supplementary Figure S7A). In co-IP experiments, binding of SPP1 to ITGAV and ITGB5 was confirmed in *ITGB1*-silenced HCC cells following CAF-CM treatment; SPP1 also bound to ITGB1, ITGB5, and ITGAV in *ITGB5*-silenced HCC cells; in HCC cells deficient for both ITGB1 and ITGB5, binding of SPP1 to integrins was not detected (Figure 5D). Treatment with SPP1-BP disrupted the binding of SPP1 to integrins on HCC cells (Figure 5E). Our results confirm that CAF-derived SPP1 binds to integrin $\alpha V\beta 5$, $\alpha 5\beta 1$, and $\alpha V\beta 1$ on HCC cells.

Genetic silencing experiments demonstrated that CAF-CM-induced resistance to sorafenib and lenvatinib was dependent on the expression of *ITGB1* and *ITGB5*. In CAF-CM-treated HCC cells, treatment of TKIs did not affect cell growth, proliferation, viability, and caspase 3/7 activity. However, under silencing of *ITGB1* and/or *ITGB5*, these parameters were significantly changed depending on treatment of TKIs, even in CAF-CM-treated HCC cells (Supplementary Figure S7B-E).

3.9 | Clinical implication of ITGB1 and ITGB5 expression in publicly available datasets

Subsequently, we compared the expression of *ITGB1* and *ITGB5* between sorafenib responders and non-responders using the GSE109211 and GSE143233 datasets

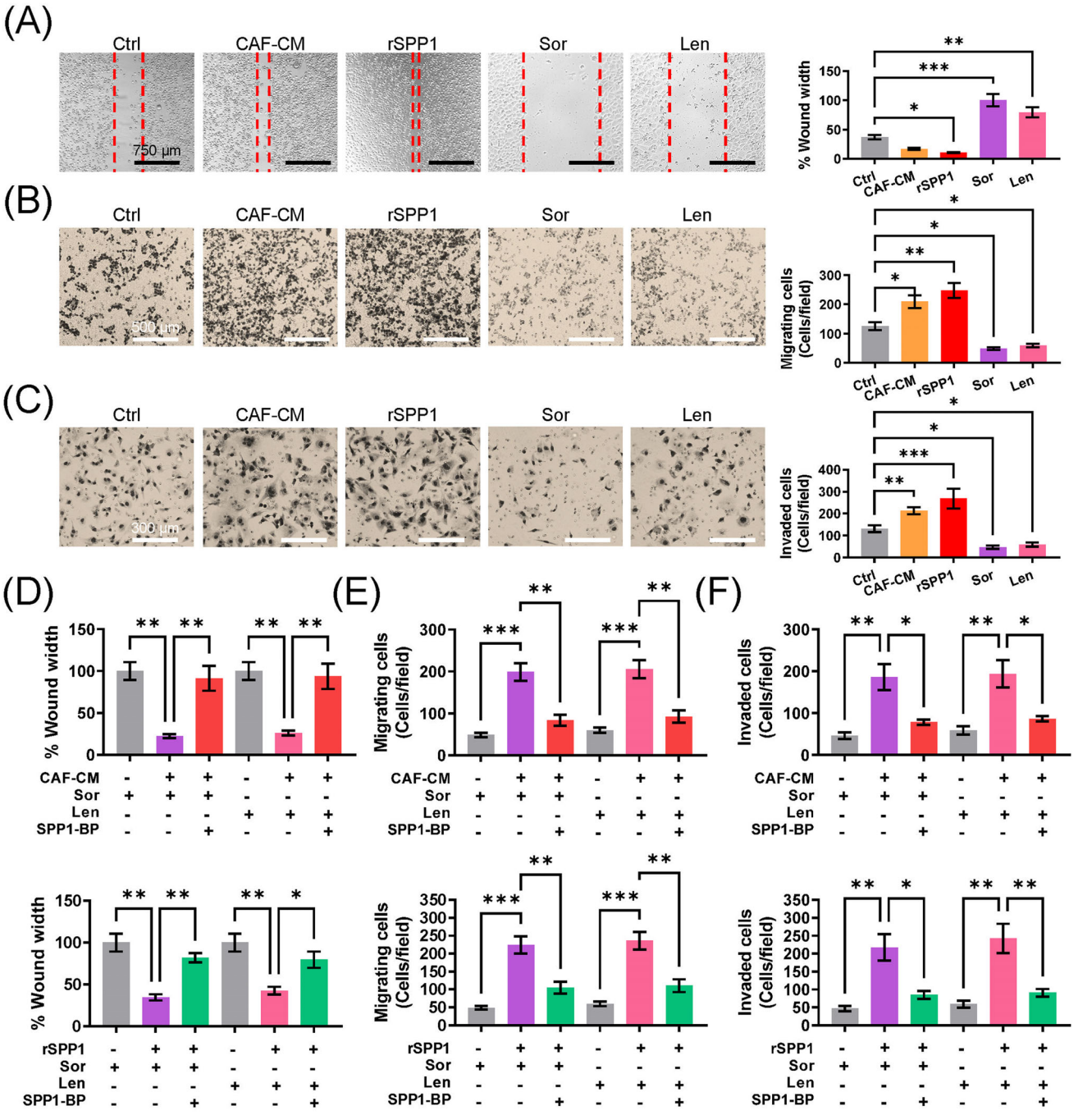

FIGURE 3 Effect of CAF-derived SPP1 and SPP1-BP on HCC sensitivity to sorafenib or lenvatinib in terms of wound healing, migration, and invasion. (A-F) Changes in the capacity for wound healing (A, D), migration (B, E), and invasion (C, F) in Huh-7 cells treated with CAF-CM, rSPP1, sorafenib (15 μmol/L), lenvatinib (5 μmol/L), and SPP1-BP alone or in different combinations. (Mean ± SEM; One-way ANOVA test; *$P < 0.05$; **$P < 0.01$; ***$P < 0.001$).

Abbreviations: Ctrl, control; CAF, cancer-associated fibroblast; CM, culture medium; rSPP1, recombinant SPP1; Sor, sorafenib; Len, lenvatinib; SPP1-BP, SPP1-blocking peptide.

(Supplementary Figure S8A). As expected, *ITGB1* and *ITGB5* demonstrated significantly higher expression in sorafenib non-responders in the GSE109211. In the GSE143233, the expression of *ITGB1* and *ITGB5* was also higher in sorafenib non-responders than in sorafenib responders. However, this difference was not statistically significant, because the GSE143233 included only six subjects.

Correlations between the expression of *SPP1* and *ITGB1*/*ITGB5* were analyzed. As expected, *SPP1* and

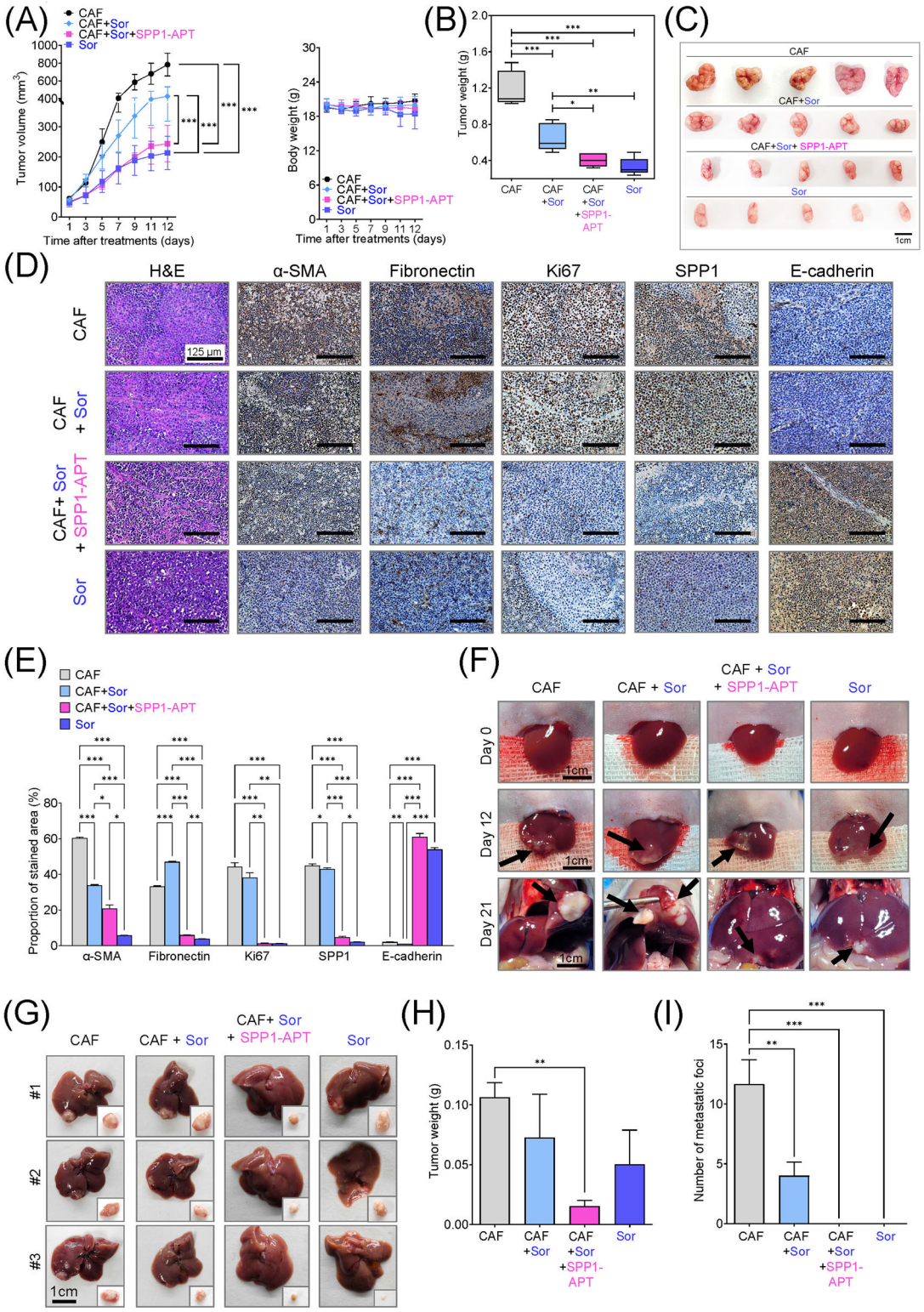

FIGURE 4 Effect of CAFs and SPP1 aptamer on HCC resistance to sorafenib in vivo. (A) Changes in tumor volume (left) and body weight (right) during sorafenib treatment. (B-C) Comparison of tumor weight between the groups (B) and macrograph of resected tumors (C). (D) H&E and IHC staining of α-SMA, Fibronectin, Ki67, SPP1, and E-cadherin in the tumor sections. (E) Comparison of IHC staining intensity for α-SMA, Fibronectin, Ki67, SPP1, and E-cadherin between the groups. (F) Representative images of liver and orthotopic tumors in each group on day 0, 12, and 21 after cell injection. (G) Representative images of orthotopic tumors in each group. (H) Comparison of orthotopic tumor weight between the groups. (I) Comparison of the intrahepatic metastatic foci number between the groups. (Mean ± SEM; Two-way ANOVA test; $^{*}P < 0.05$; $^{**}P < 0.01$; $^{***}P < 0.001$).

Abbreviations: CAF, cancer-associated fibroblast; Sor, sorafenib; SPP1-APT, SPP1-aptamer; H&E, hematoxylin and eosin; α-SMA, alpha smooth muscle actin; SPP1, secreted phosphoprotein 1.

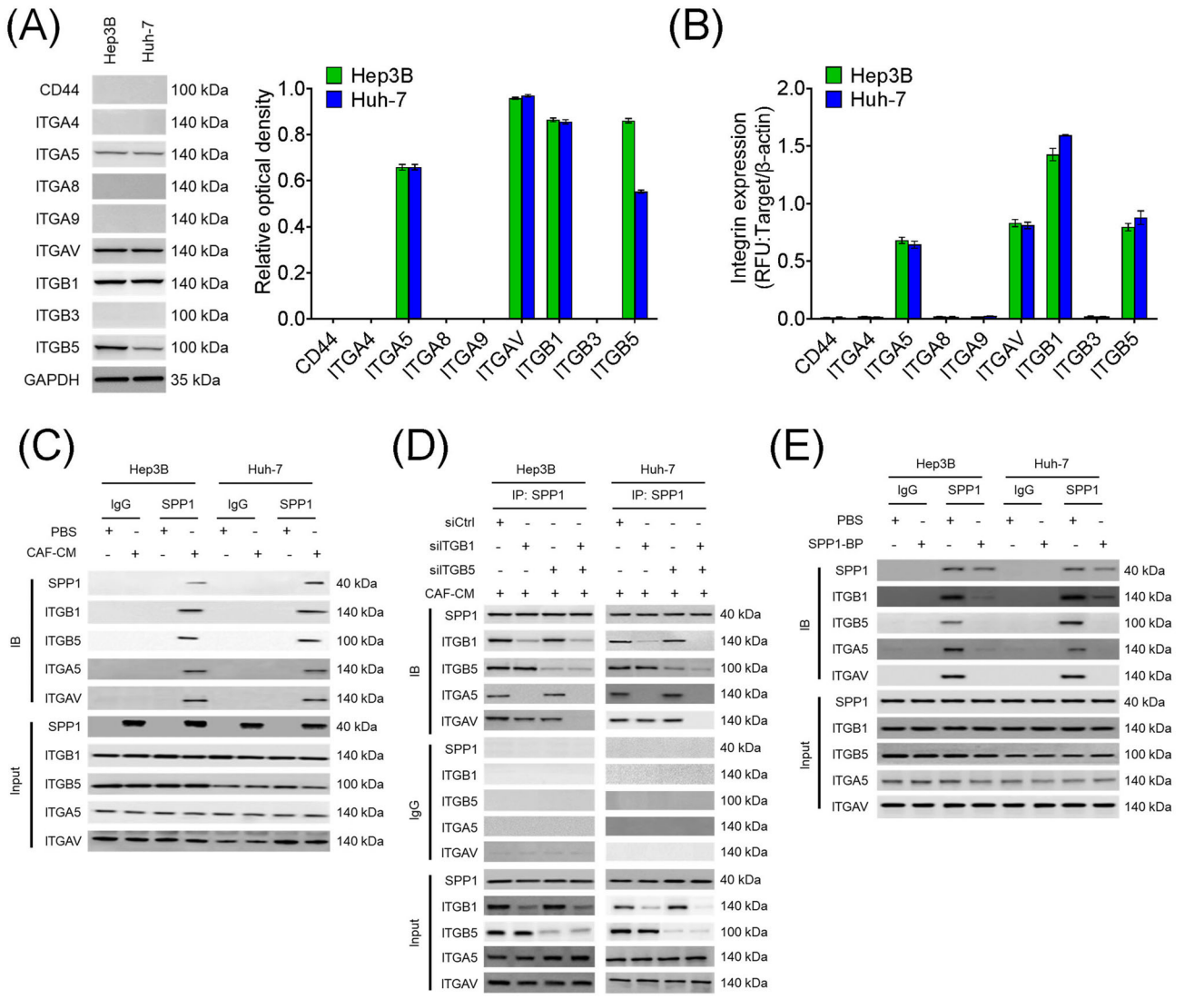

FIGURE 5 Integrin complexes (integrin αVβ5, α5β1, and αVβ1) on HCC cells were identified as binding proteins of SPP1. (A) Western blotting of SPP1 receptor-binding protein expression in HCC cells. (B) Measurement of CD44 and integrin expression in Hep3B and Huh-7 cells by fluorescent intensity. (C-E) Co-IP of SPP1 after CAF-CM treatment, followed by Western blotting for SPP1, ITGA5, ITGAV, ITGB1, and ITGB5 in HCC cells (C), HCC cells silenced for *ITGB1* and/or *ITGB5* (D), and HCC cells incubated with/without SPP1-BP (E).
Abbreviations: ITGA4, integrin subunit α4; ITGA5, integrin subunit α5; ITGA8, integrin subunit α8; ITGA9, integrin subunit α9; ITGAV, integrin subunit αV; ITGB1, integrin subunit β1; ITGB3, integrin subunit β3; ITGB5, integrin subunit β; GAPDH, glyceraldehyde 3-phosphate dehydrogenase; RFU, relative fluorescence units; IgG, immunoglobulin G; SPP1, secreted phosphoprotein 1; CAF, cancer-associated fibroblast; CM, culture medium; IB, immunoblotting; siCtrl, negative control; SPP1-BP, SPP1-blocking peptide.

ITGB1/*ITGB5* expression showed positive correlations both in TCGA LIHC and GSE109211 datasets (Supplementary Figure S8B).

Moreover, survival analysis according to *ITGB1*/*ITGB5* and *SPP1* expression was performed in 371 patients with HCC in the TCGA LIHC cohort. These patients were divided into two groups according to the median values of *SPP1, ITGB1*, and *ITGB5* expression. Patients with high *SPP1, ITGB1*, and *ITGB5* expression had significantly shorter OS and DFS than those with low expression (OS, log-rank $P < 0.001$, hazard ratio [HR] = 3.02; DFS, log-rank $P = 0.034$, HR = 1.67) (Supplementary Figure S8C).

3.10 | CAF-derived SPP1 activated the RAF/ERK/STAT3 and PI3K/AKT/mTOR signaling pathways via PKCα phosphorylation in HCC cells

Prior studies have shown that TKIs, including sorafenib and lenvatinib, suppressed tumor progression by inhibit-

ing the RAF/MAPK/STAT3 and PI3K/AKT/mTOR signaling pathways via targeting RTKs [26–28]. Cytoscape analysis indicated that the SPP1 signaling pathway is initiated by the SPP1-integrin interaction, subsequently activating MAPK and AKT pathways via the activation of PKCα (Supplementary Figure S9). Therefore, we hypothesized that CAF-derived SPP1 induces resistance to TKIs through bypass activation of the RAF/ERK/STAT3 and PI3K/AKT/mTOR pathways via integrin-mediated PKCα phosphorylation. In Western blotting, treatment with sorafenib or lenvatinib was shown to significantly inhibit the phosphorylation of BRAF/ERK/STAT3 and PI3K/AKT/mTOR pathways in HCC cells, while PKCα phosphorylation was not affected (Supplementary Figure S10A). The phosphorylation of PKCα, BRAF/ERK/STAT3, and PI3K/AKT/mTOR was significantly upregulated in HCC cells treated with CAF-CM (Figure 6A-B). Similar results were observed when HCC cells were treated with rSPP1 (Supplementary Figure S10B). When HCC cells were incubated with CAF-CM or rSPP1, the phosphorylation of PKCα/BRAF/ERK/STAT3 and PI3K/AKT/mTOR was slightly affected by sorafenib or lenvatinib treatment. However, when cells were treated with SPP1-BP, the phosphorylation of PKCα, BRAF/ERK/STAT3, and PI3K/AKT/mTOR was markedly inhibited by TKIs even under incubation with CAF-CM or rSPP1 (Figure 6A-B and Supplementary Figure S10B). We also evaluated TKI-induced changes in PKCα, BRAF/ERK/STAT3, and PI3K/AKT/mTOR phosphorylation under *ITGB1* and/or *ITGB5* silencing. When HCC cells were transfected with *siITGB1* and/or *siITGB5*, phosphorylation of PI3K/AKT/mTOR and BRAF/ERK/STAT3 in HCC cells were markedly reduced by TKI treatment even after incubation with CAF-CM (Figure 6C-D). Overall, these findings indicate that CAF-derived SPP1 induces TKI resistance to bypass activation of the RAF/ERK/STAT3 and PI3K/AKT/mTOR signaling pathways through integrin-mediated PKCα phosphorylation.

3.11 | SPP1-related gene signatures indicated poor prognosis in patients with HCC

We examined the clinical relevance of *SPP1* expression in HCC tissues using data from TCGA LIHC. *SPP1* was significantly upregulated in HCC tissues compared to non-tumor tissues in TCGA LIHC dataset, and *SPP1* expression was found to gradually increase with higher histologic grade and clinical status of liver disease (Figure 7A). Patients with high *SPP1* expression displayed short OS and DFS (OS, log-rank $P < 0.001$, HR = 2.02; DFS, log-rank $P = 0.024$, HR = 1.41; Figure 7B). We subsequently assessed *SPP1*-related gene signatures. The gene sets that were highly correlated with *SPP1* ($P < 0.001$; $r \geq 0.3$ or $r \leq 0.3$) were selected as the *SPP1*-related gene signature ($n = 1{,}601$). In the TCGA LIHC dataset, patients with HCC could be categorized into two clusters according to expression patterns of the SPP1-related gene sets (Figure 7C, left). The cluster with a high expression of SPP1-related genes had significantly shorter OS and DFS compared to that with a low expression (OS, log-rank $P < 0.001$, HR = 2.03; DFS, log-rank $P = 0.003$, HR = 1.58; Figure 7C, right). These results suggest that the expression of *SPP1*-related gene signatures is significantly related with the prognosis in patients with HCC.

3.12 | CAF-derived SPP1 promoted the EMT of HCC cells

SPP1-related gene signatures were enriched in a variety of cancer-associated pathways (Figure 7D). Among these, the EMT-associated gene set was the most highly enriched. The expression levels of four EMT-related genes (*ITGAV, NTM, COMP*, and *FAP*), which were randomly selected from the EMT gene set, exhibited a high correlation with *SPP1* expression in TCGA LIHC (Supplementary Figure S11A). On Western blotting and relative densitometry bar graphs (Supplementary Figure S11B), Vimentin and Snail were downregulated after sorafenib or lenvatinib treatment, in parallel to significantly increased E-cadherin expression. However, the expression of EMT-related proteins in HCC cells treated with CAF-CM or rSPP1 was not affected by TKI treatment. Further, SPP1-BP treatment completely reversed the effects of CAF-CM and rSPP1 on EMT-related protein expression.

3.13 | EMT-related genes were specifically expressed in SPP1-positive fibroblasts

To assess differences in *SPP1* expression across distinct fibroblast subpopulations, we processed and analyzed a publicly available single-cell RNA-seq dataset derived from patients with HCC (GSE151530). We identified seven cell types from the 56,721 QC-filtered cells (Figure 7E), among which fibroblasts were further clustered into six cell clusters, denoted as C0 to C5 (Figure 7F-G). Notably, *SPP1* was predominantly expressed in cells of C4 (Figure 7H). Thus, we used the 'MSigDB Hallmark' database to identify the molecular signature of C4 fibroblasts; EMT appeared as the most enriched term (Figure 7I). We verified this in another publicly available single-cell RNA-seq dataset from patients with malignant liver

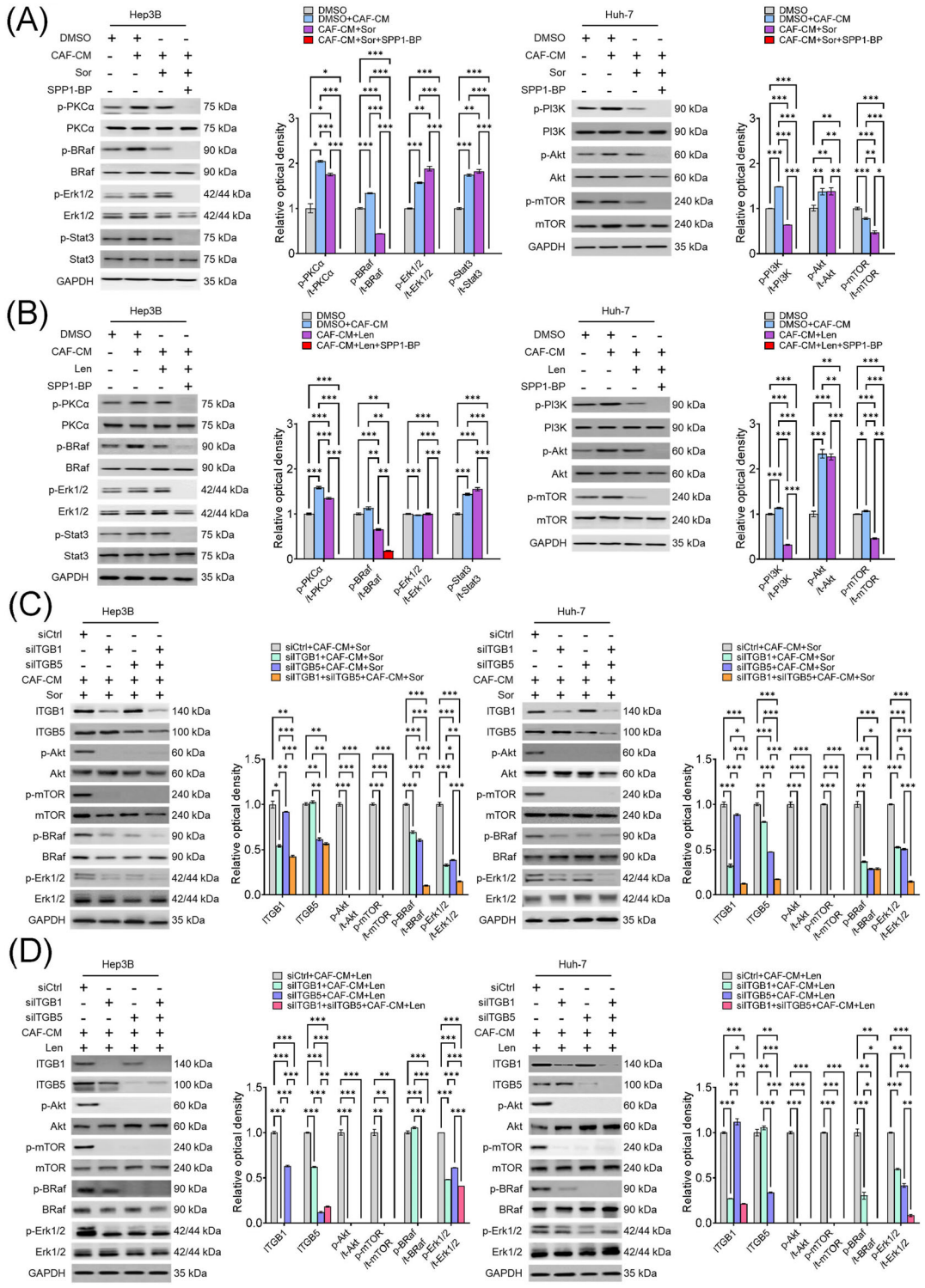

FIGURE 6 Molecular mechanism underlying CAF-derived SPP1-induced resistance to sorafenib or lenvatinib. (A-B) Changes in the expression levels of PKCα, BRAF/ERK/STAT3, and PI3K/AKT/mTOR pathway proteins in CAF-CM-incubated Huh-7 cells treated with sorafenib (15 μmol/L; A) or lenvatinib alone (5 μmol/L; B) and in combination with SPP1-BP. (C-D) Changes in the phosphorylation of AKT, mTOR, BRAF, and ERK1/2 under *ITGB1* and/or *ITGB5* silencing in Hep3B and Huh-7 cells treated with sorafenib (C) or lenvatinib (D) in combination with CAF-CM. (Mean ± SEM; Two-way ANOVA test; *$P < 0.05$; **$P < 0.01$; ***$P < 0.001$).

Abbreviations: DMSO, dimethyl sulfoxide; CAF, cancer-associated fibroblast; CM, culture medium; Sor, sorafenib; SPP1-BP, SPP1-blocking peptide, PKCα, protein kinase C α; BRAF,v-Raf murine sarcoma viral oncogene homolog B; ERK, extracellular signal-related kinase; STAT3, signal transducer and activator of transcription 3; GAPDH, glyceraldehyde 3-phosphate dehydrogenase; PI3K, phosphatidylinositol-3-kinase; AKT, protein kinase B; mTOR, mammalian target of rapamycin; Len, lenvatinib; siCtrl, negative control; ITGB1, integrin subunit β1; ITGB5, integrin subunit β5.

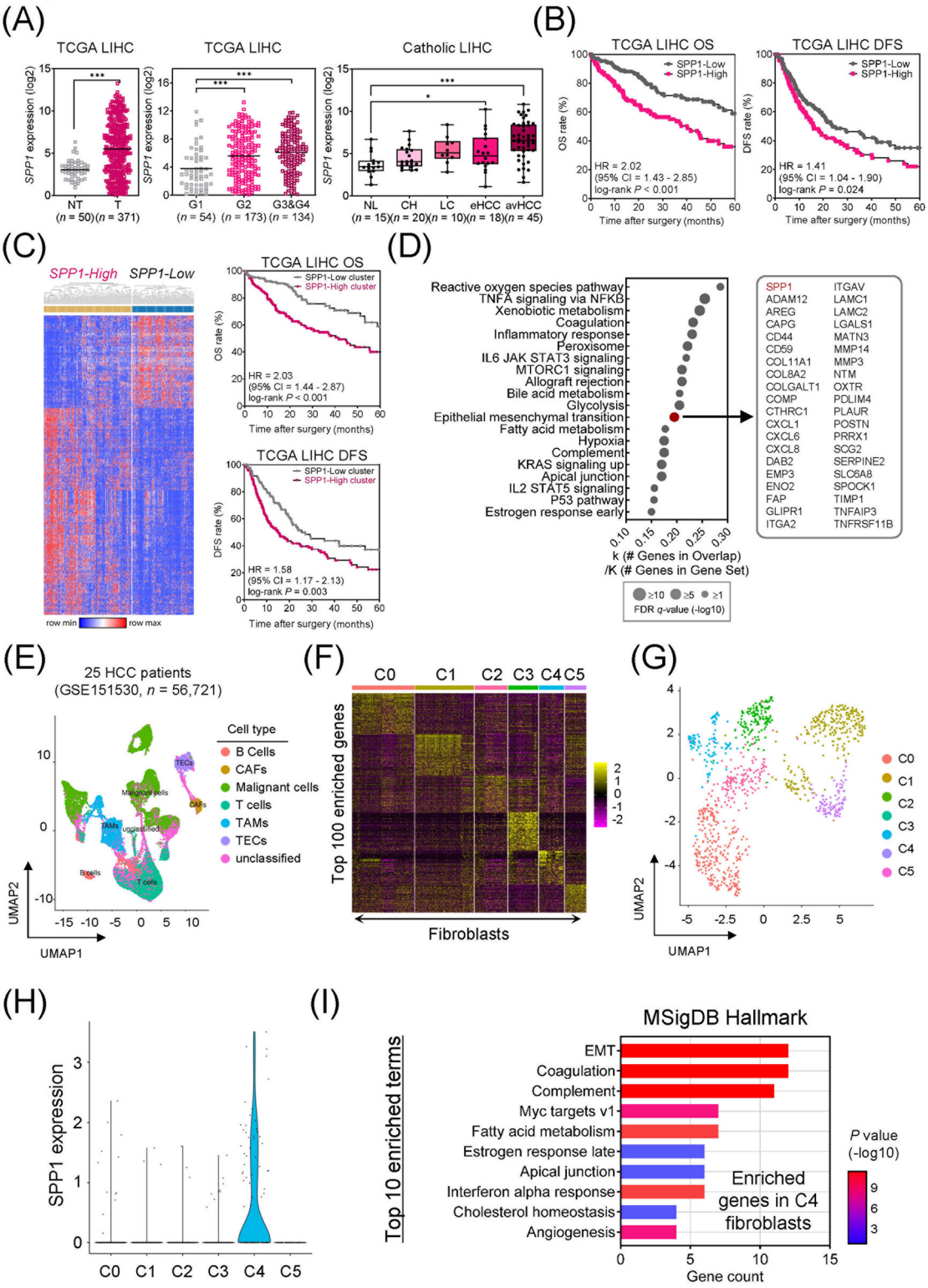

FIGURE 7 Prognostic relevance of *SPP1* expression in TCGA LIHC data and enrichment of EMT-related genes in the *SPP1*-positive CAF cluster in GSE151530. (A) *SPP1* expression in HCC and adjacent non-tumor tissues of TCGA LIHC (left), *SPP1* expression according to histologic grade and clinical status of liver disease in TCGA LIHC (middle) and Catholic LIHC (right). (B) Kaplan-Meier plots of OS (left) and DFS (right) based on *SPP1* expression in TCGA LIHC. (C) Heatmap of *SPP1*-related genes in TCGA LIHC (left). Comparison of OS and DFS between clusters divided by *SPP1*-related gene expression patterns (right). (D) GSEA of SPP1-related gene signatures. (E) UMAP plot depicting cells of the human HCC microenvironment. (F) Expression heatmap of the top 100 enriched genes in subclusters of fibroblasts (C0 to C5). (G) UMAP plot visualizing subclusters of fibroblasts. (H) Violin plot showing SPP1 expression levels in fibroblast subclusters. (I) Bar graph

cancer such as metastatic liver cancer or cholangiocarcinoma (GSE146409). Of the 17 cell types (Supplementary Figure S11C), fibroblasts were further clustered into five cell clusters, and *SPP1* expression was predominant in C2 cells (Supplementary Figure S11D-F). The EMT appeared again as the top enriched term in C2 fibroblasts via the 'MSigDB Hallmark' database analysis (Supplementary Figure S11G).

3.14 | Plasma SPP1 level prior to sorafenib or lenvatinib treatment was an independent predictor of PFS or OS in patients with advanced HCC

We subsequently investigated whether plasma SPP1 levels before sorafenib or lenvatinib treatment initiation would be a useful prognostic biomarker for predicting PFS or OS in patients with advanced HCC. The baseline characteristics of included patients ($n = 54$) are presented in Supplementary Table S4. Among the 54 patients, 36 were treated with sorafenib, while 18 were treated with lenvatinib. Six patients had a partial response (PR) to treatment, 25 had stable disease (SD), and 23 demonstrated progressive disease (PD; Figure 8A). Representative CT scans of patients who achieved PR to TKI are demonstrated in Figure 8B. Supplementary Figure S11H shows that plasma SPP1 levels were significantly higher in patients with PD than in those with PR or SD.

Of the included patients, those with high plasma SPP1 levels (> 2,300 pg/mL, $n = 28$) had significantly shorter PFS and OS compared to those with low plasma SPP1 levels (≤ 2,300 pg/mL, $n = 26$) (PFS, log-rank $P < 0.001$, Figure 8C, left; OS, log-rank $P = 0.002$; Figure 8D, left). In the subgroup treated with sorafenib ($n = 36$), patients with high plasma SPP1 levels exhibited shorter PFS and OS (PFS, log-rank $P = 0.005$, Figure 8C, middle; OS, log-rank $P = 0.007$, Figure 8D, middle). Moreover, in the lenvatinib subgroup ($n = 18$), patients with high plasma SPP1 levels had significantly shorter PFS (log-rank $P = 0.011$, Figure 8C, right) and OS (Breslow $P = 0.037$, Figure 8D, right).

In univariate Cox regression analysis, large tumor size (> 10 cm) and high plasma SPP1 (> 2,300 pg/mL) were identified as significant risk factors for both PFS and OS. In multivariate analysis, only a high plasma SPP1 level was identified as an independent risk factor for predicting poor PFS in both model 1 and model 2 in (model 1, $P = 0.026$, HR = 2.48, 95% confidence interval [CI] = 1.11-5.53; model 2, $P = 0.022$, HR = 2.96, 95% CI = 1.17-7.51) and as an independent risk factor of poor OS only in model 1 ($P = 0.047$, HR = 2.54, 95% CI = 1.01-6.35) (Supplementary Table S5).

4 | DISCUSSION

Resistance to systemic therapeutics is a major hurdle in the treatment of advanced HCC [29]. Sorafenib and lenvatinib, which exert their anticancer effect by suppressing the RAF/ERK/STAT3 and PI3K/AKT/mTOR pathways via RTK inhibition, have been the standard first-line systemic therapy for advanced HCC. Various studies have investigated the mechanisms underlying HCC resistance to TKIs in an attempt to identify novel therapeutic targets to overcome resistance [30, 31]. In the present study, we determined that CAF-derived SPP1 played a key role in inducing TKI resistance in HCC. That is, CAFs secreted SPP1, which bound to the extracellular domain of integrin complexes (integrin $\alpha V\beta 5$, $\alpha 5\beta 1$, and $\alpha V\beta 1$) on HCC cells, subsequently phosphorylating PKCα in the cytoplasmic domain. This, in turn, activated the RAF/ERK/STAT3 and PI3K/AKT/mTOR pathways, driving TKI resistance. Treatment with SPP1 inhibitors, such as SPP1-BP or SPP1-APT, reversed CAF-induced resistance to sorafenib or lenvatinib, suggesting CAF-derived SPP1 as a novel therapeutic target for overcoming TKI resistance in HCC (Figure 9).

In addition to the SPP1-induced activation of oncogenic signal bypass, we demonstrated that CAF-derived SPP1 could promote EMT. EMT plays a crucial role in cancer cell metastasis and invasion [32]. Moreover, it has been described as an important driver of TKI resistance in HCC [33, 34]. Thus, targeting EMT could represent a strategy for overcoming drug resistance. Mir *et al.* [34] reported that the combination of EMT inhibitors and sorafenib improved the sensitivity of HCC cells to sorafenib. In the present study, *SPP1* expression was highly correlated with that of EMT-related genes in TCGA LIHC (Supplementary Figure S11A). EMT was equally the most enriched term of the *SPP1*-positive CAF cluster (Figure 7I). Fur-

showing the top 10 enriched terms in C4 fibroblasts using the 'MSigDB Hallmark' database. (Mean ± SEM; One-way ANOVA test; *$P < 0.05$; **$P < 0.01$; ***$P < 0.001$).

Abbreviations: SPP1, secreted phosphoprotein 1; TCGA LIHC, The Cancer Genome Atlas liver hepatocellular carcinoma project; Catholic LIHC, Catholic University of Korea's liver hepatocellular carcinoma project; NT, non-tumor; T, tumor; NL, normal liver; CH, chronic hepatitis; LC, liver cirrhosis; eHCC, early HCC; avHCC, advanced HCC; OS, overall survival; DFS, disease free survival; HR, hazard ratio; CI, confidence interval; UMAP, Uniform manifold approximation and projection; CAFs, cancer-associated fibroblasts; TAMs, Tumor-associated macrophages; TECs, thymic epithelial cells; MSigDB, the Molecular Signatures Database.

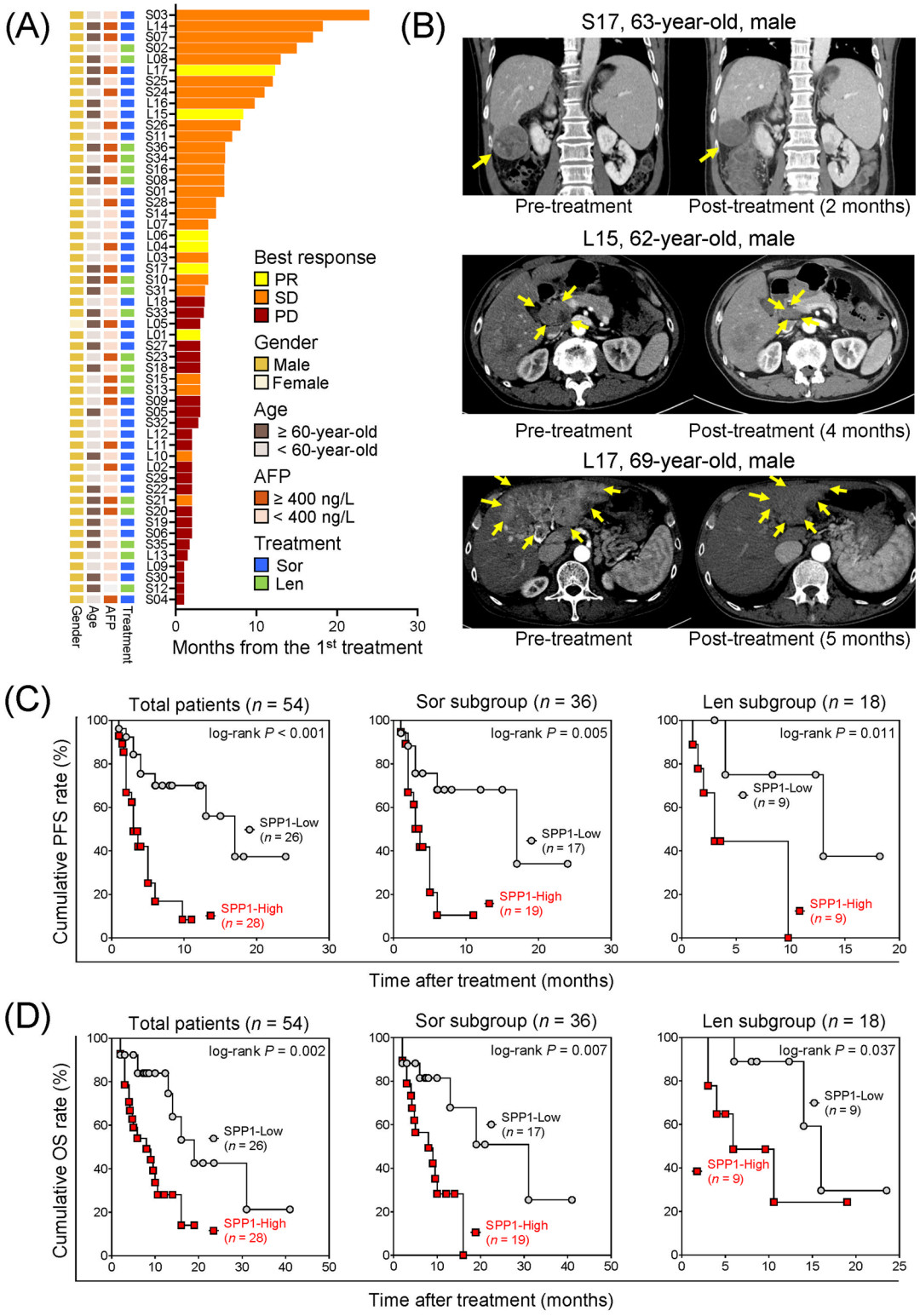

FIGURE 8 Clinicopathological features in association with response to sorafenib and lenvatinib and Kaplan-Meier analysis of PFS and OS as per plasma SPP1 levels in patients with HCC treated with sorafenib or lenvatinib. (A) Swimmer plot of time on treatment for enrolled patients ($n = 54$). Individual patient data are presented by each lane. (B) Computed tomography image of three responders showing tumor reduction after sorafenib or lenvatinib treatment. (C) PFS according to plasma SPP1 levels in all included patients ($n = 54$, left), patients treated with sorafenib ($n = 36$, middle), and patients treated with lenvatinib ($n = 18$, right). (D) OS according to plasma SPP1 levels in all included patients ($n = 54$, left), patients treated with sorafenib ($n = 36$, middle), and lenvatinib ($n = 18$, right).

Abbreviations: PR, partial response; SD, stable disease; PD, progressive disease; AFP, alpha-fetoprotein; Sor, sorafenib; Len, lenvatinib; PFS, progression free survival; OS, overall survival.

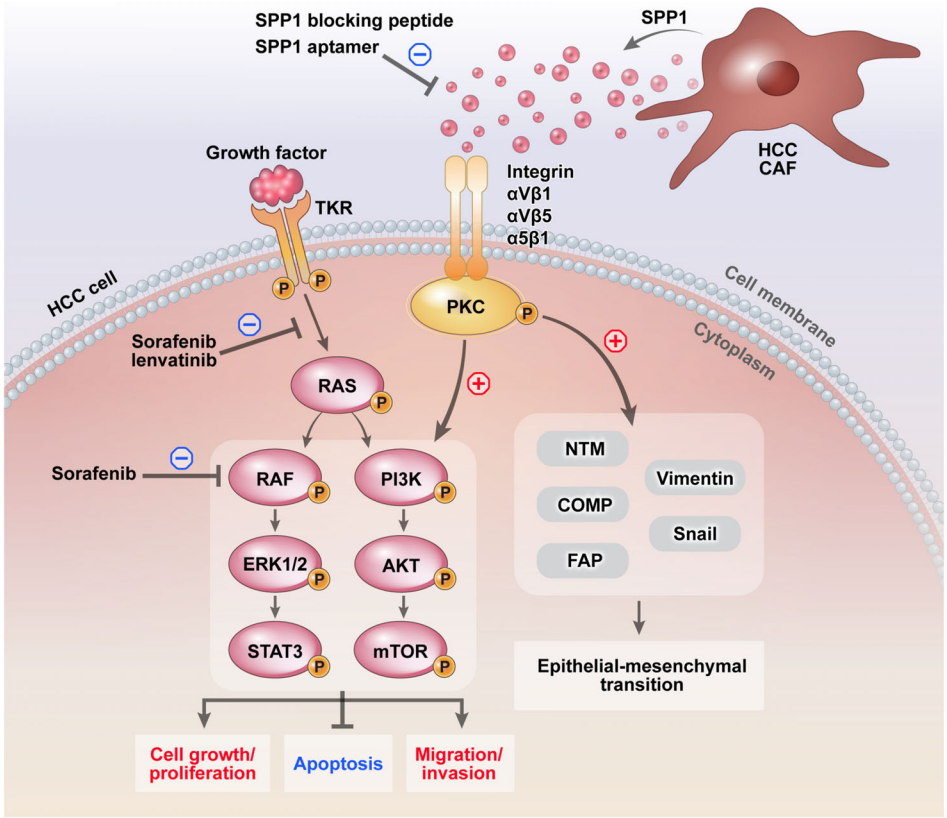

FIGURE 9 Schematic diagram illustrating the mechanism of CAF-derived SPP1 in HCC resistance to sorafenib/lenvatinib. Abbreviations: SPP1, secreted phosphoprotein 1; HCC, hepatocellular carcinoma; CAF, cancer-associated fibroblast; TKR, receptor tyrosine kinase; PKC, protein kinase C; RAF, rapidly accelerated fibrosarcoma; PI3K, phosphatidylinositol-3-kinase; ERK, extracellular signal-related kinase; AKT, protein kinase B; STAT3, signal transducer and activator of transcription 3; mTOR, mammalian target of rapamycin; NTM, neurotrimin; COMP, cartilage oligomeric matrix protein; FAP, fibroblast activation protein alpha.

ther, CAF-derived SPP1 promoted the EMT by regulating EMT-related gene expression in vitro and in vivo (Supplementary Figure S11B and Figure 4D). Taken together, these results suggest that CAF-derived SPP1 promotes the EMT in HCC. Several previous studies have similarly shown that SPP1 promoted a stem cell-like phenotype as well as EMT in HCC [35–37]. Thus, the combination of SPP1-blocking agents with sorafenib or lenvatinib represents a promising therapeutic strategy for overcoming TKI resistance in HCC via suppression of the SPP1-mediated EMT and SPP1-integrin-PKCα bypass signaling pathways.

SPP1, also known as osteopontin, is encoded by the *SPP1* gene in humans. SPP1 is known as an integrin-binding glycoprotein, which is overexpressed in various types of cancers, including HCC [38]. Moreover, the overexpression of SPP1 in cancer tissues is considered to be associated with poor prognosis [39]. Several previous studies have described the oncogenic properties of SPP1 [40–42]. However, the major source of SPP1 within the HCC TME remained unclear. Thus, we sought to elucidate the major source of secretory SPP1. SPP1 was significantly overexpressed in CAF cell lysates and CAF-CM, when compared to CM and lysates of other cells, including HCC cells, paracancer fibroblasts, and NFs (Supplementary Figure S2D). Further, IF staining confirmed co-localization of α-SMA and SPP1 in the tumor stroma. In addition, IHC analysis indicated that SPP1 was markedly overexpressed in the tumor stroma compared to non-neoplastic fibrous tissue or other tumor tissues. These results suggest CAFs as the major source of secretory SPP1 within the HCC TME. Similarly, several recent studies demonstrated that CAFs secrete SPP1, which plays an essential oncogenic role in several different malignancies [43, 44].

Currently, there are no reliable biomarkers for predicting the response to sorafenib or lenvatinib treatment in patients with HCC. In several previous studies, circulating SPP1 has shown promise as a diagnostic and prognostic biomarker in HCC [45–47]. However, its relevance as a prognostic biomarker in patients with advanced-stage HCC receiving sorafenib or lenvatinib has not yet been evaluated. Based on our results of SPP1 being a secretory protein found to play a key role in TKI resistance, we hypothesized that circulating SPP1 levels may be associated with sorafenib and lenvatinib treatment response.

Consequently, a high plasma SPP1 level was identified as an independent risk factor for predicting poor PFS and poor OS in patients with HCC receiving TKIs.

Meanwhile, the present study had some limitations. First, the in vivo orthotopic xenograft model used in this study was the BALB/c female nude mice which could not reflect the tumor-immune microenvironment. Although we demonstrated CAF-derived SPP1 as an important mechanism of TKI resistance of HCC cells, TKI resistance may also have other mechanisms, such as CAF-immune cell interaction. Thus, 3-dimensional in vitro model of HCC or in vivo experiments using immune-competent animal model would be more helpful to understand the complex mechanism of TKI resistance in patients with HCC. Second, although we showed the prognostic implication of plasma SPP1 in patients with advanced HCC, this study included a relatively small number of patients with HCC in a retrospective manner. To confirm the clinical significance of plasma SPP1 as a prognostic biomarker in patients with advanced HCC planned for TKI treatment, the current findings should be subjected to further validation in a larger external cohort.

5 | CONCLUSIONS

In summary, we reported that CAF-derived SPP1 induced TKI resistance in HCC. SPP1 blockade could represent a potential therapeutic strategy for overcoming resistance to sorafenib or lenvatinib in HCC. Consistently, a high plasma SPP1 level before TKI treatment was associated with poor prognosis of HCC patients, demonstrating that it may be a potential prognostic biomarker for patients with advanced HCC planned for TKI treatment.

DECLARATIONS

AUTHOR CONTRIBUTIONS

JWE, HJC and JYC made substantial contributions to the conception and design of the present study. JHY, HRA, JHW and GOB performed the in vitro experiments. JAS and MGY performed the in vivo experiments. JWE, SBL, WP, and TWK acquired and analyzed the data. SK and YBK interpreted all the datasets in the present study. JHY, HRA and HJC drafted the initial manuscript and critically revised it for important intellectual content. JWE, SSK and JYC confirmed the authenticity of all the raw data. All authors have read and approved the final manuscript.

AFFILIATIONS

[1]Department of Gastroenterology, Ajou University School of Medicine, Suwon, South Korea

[2]Department of Pathology, College of Medicine, The Catholic University of Korea, Seoul, South Korea

[3]Department of Biomedical Sciences, Ajou University Graduate School of Medicine, Suwon, South Korea

[4]Department of Pathology, Ajou University School of Medicine, Suwon, South Korea

[5]Department of Biochemistry & Molecular Biology, Ajou University School of Medicine, Suwon, South Korea

[6]The Moagen, Inc, Daejeon, South Korea

ACKNOWLEDGEMENTS

The biospecimens and data used for this study were provided by the Biobank of Ajou University Hospital, a member of the Korea Biobank Network. This research was supported by grants from the Korea Health Technology R&D Project through the Korea Health Industry Development Institute, funded by the Ministry of Health and Welfare, Republic of Korea (HR21C1003, HR22C1734), as well as the Bio and Medical Technology Development Program of the National Research Foundation (NRF-2021R1C1C1009619 and NRF-2022R1A2C2092422), funded by the Korean government (Ministry of Science and Information & Communications Technology).

CONFLICT OF INTEREST STATEMENT

The authors have declared that no conflict of interest exists.

CONSENT FOR PUBLICATION

Not applicable.

DATA AVAILABILITY STATEMENT

RNA-sequencing datasets generated in this study are deposited in the Gene Expression Omnibus database under accession code GSE192912. All other supporting data are available from the corresponding author upon reasonable request.

ETHICS APPROVAL AND CONSENT TO PARTICIPATE

All experiments were performed according to the Declaration of Helsinki and the study was approved by the Institutional Review Board (AJIRB-BMR-SMP-17-188). All animal experiments were performed according to the Guide for the Care and Use of Laboratory Animals. The experiments were approved by the Ethics Committee for Laboratory Animal Research Center of Ajou University Medical Center (IACUC-2020-0038).

ORCID

Jung Hwan Yoon https://orcid.org/0000-0001-7770-2965
Hyo Jung Cho https://orcid.org/0000-0003-4792-8335

REFERENCES

1. Yang JD, Hainaut P, Gores GJ, Amadou A, Plymoth A, Roberts LR. A global view of hepatocellular carcinoma: trends, risk, prevention and management. Nat Rev Gastroenterol Hepatol. 2019;16(10):589-604.
2. European Association for the Study of the Liver. Electronic address eee, European Association for the Study of the L. EASL Clinical Practice Guidelines: Management of hepatocellular carcinoma. J Hepatol. 2018;69(1):182-236.
3. Llovet JM, Villanueva A, Marrero JA, Schwartz M, Meyer T, Galle PR, et al. Trial Design and Endpoints in Hepatocellular Carcinoma: AASLD Consensus Conference. Hepatology. 2021;73 Suppl 1:158-91.
4. Cheng AL, Hsu C, Chan SL, Choo SP, Kudo M. Challenges of combination therapy with immune checkpoint inhibitors for hepatocellular carcinoma. J Hepatol. 2020;72(2):307-19.
5. Faivre S, Rimassa L, Finn RS. Molecular therapies for HCC: Looking outside the box. J Hepatol. 2020;72(2):342-52.
6. Sharma R, Motedayen Aval L. Beyond First-Line Immune Checkpoint Inhibitor Therapy in Patients With Hepatocellular Carcinoma. Front Immunol. 2021;12:652007.
7. Doycheva I, Thuluvath PJ. Systemic Therapy for Advanced Hepatocellular Carcinoma: An Update of a Rapidly Evolving Field. J Clin Exp Hepatol. 2019;9(5):588-96.
8. Kudo M, Finn RS, Qin S, Han KH, Ikeda K, Piscaglia F, et al. Lenvatinib versus sorafenib in first-line treatment of patients with unresectable hepatocellular carcinoma: a randomised phase 3 non-inferiority trial. Lancet. 2018;391(10126):1163-73.
9. Cheng AL, Kang YK, Chen Z, Tsao CJ, Qin S, Kim JS, et al. Efficacy and safety of sorafenib in patients in the Asia-Pacific region with advanced hepatocellular carcinoma: a phase III randomised, double-blind, placebo-controlled trial. Lancet Oncol. 2009;10(1):25-34.
10. Liu T, Zhou L, Li D, Andl T, Zhang Y. Cancer-Associated Fibroblasts Build and Secure the Tumor Microenvironment. Front Cell Dev Biol. 2019;7:60.
11. Karagiannis GS, Poutahidis T, Erdman SE, Kirsch R, Riddell RH, Diamandis EP. Cancer-associated fibroblasts drive the progression of metastasis through both paracrine and mechanical pressure on cancer tissue. Mol Cancer Res. 2012;10(11):1403-18.
12. Kubo N, Araki K, Kuwano H, Shirabe K. Cancer-associated fibroblasts in hepatocellular carcinoma. World J Gastroenterol. 2016;22(30):6841-50.
13. Fiori ME, Di Franco S, Villanova L, Bianca P, Stassi G, De Maria R. Cancer-associated fibroblasts as abettors of tumor progression at the crossroads of EMT and therapy resistance. Mol Cancer. 2019;18(1):70.
14. Peng H, Xue R, Ju Z, Qiu J, Wang J, Yan W, et al. Cancer-associated fibroblasts enhance the chemoresistance of CD73(+) hepatocellular carcinoma cancer cells via HGF-Met-ERK1/2 pathway. Ann Transl Med. 2020;8(14):856.
15. Liu J, Li P, Wang L, Li M, Ge Z, Noordam L, et al. Cancer-Associated Fibroblasts Provide a Stromal Niche for Liver Cancer Organoids That Confers Trophic Effects and Therapy Resistance. Cell Mol Gastroenterol Hepatol. 2021;11(2):407-31.
16. Yoon JH, Ham IH, Kim O, Ashktorab H, Smoot DT, Nam SW, et al. Gastrokine 1 protein is a potential theragnostic target for gastric cancer. Gastric Cancer. 2018;21(6):956-67.
17. Massalha H, Bahar Halpern K, Abu-Gazala S, Jana T, Massasa EE, Moor AE, et al. A single cell atlas of the human liver tumor microenvironment. Mol Syst Biol. 2020;16(12):e9682.
18. Marrero JA, Kulik LM, Sirlin CB, Zhu AX, Finn RS, Abecassis MM, et al. Diagnosis, Staging, and Management of Hepatocellular Carcinoma: 2018 Practice Guidance by the American Association for the Study of Liver Diseases. Hepatology. 2018;68(2):723-50.
19. Yu SJ. A concise review of updated guidelines regarding the management of hepatocellular carcinoma around the world: 2010-2016. Clin Mol Hepatol. 2016;22(1):7-17.
20. Obi S, Sato T, Sato S, Kanda M, Tokudome Y, Kojima Y, et al. The efficacy and safety of lenvatinib for advanced hepatocellular carcinoma in a real-world setting. Hepatol Int. 2019;13(2):199-204.
21. Lee JS, Choi HJ, Kim BK, Park JY, Kim DY, Ahn SH, et al. The Modified Response Evaluation Criteria in Solid Tumors (RECIST) Yield a More Accurate Prognoses Than the RECIST 1.1 in Hepatocellular Carcinoma Treated with Transarterial Radioembolization. Gut Liver. 2020;14(6):765-74.
22. Pinyol R, Montal R, Bassaganyas L, Sia D, Takayama T, Chau GY, et al. Molecular predictors of prevention of recurrence in HCC with sorafenib as adjuvant treatment and prognostic factors in the phase 3 STORM trial. Gut. 2019;68(6):1065-75.
23. Brown ZJ, Heinrich B, Greten TF. Mouse models of hepatocellular carcinoma: an overview and highlights for immunotherapy research. Nat Rev Gastroenterol Hepatol. 2018;15(9):536-54.
24. Erikson DW, Burghardt RC, Bayless KJ, Johnson GA. Secreted phosphoprotein 1 (SPP1, osteopontin) binds to integrin alpha v beta 6 on porcine trophectoderm cells and integrin alpha v beta 3 on uterine luminal epithelial cells, and promotes trophectoderm cell adhesion and migration. Biol Reprod. 2009;81(5):814-25.
25. Rodrigues LR, Teixeira JA, Schmitt FL, Paulsson M, Lindmark-Mansson H. The role of osteopontin in tumor progression and metastasis in breast cancer. Cancer Epidemiol Biomarkers Prev. 2007;16(6):1087-97.
26. Eso Y, Marusawa H. Novel approaches for molecular targeted therapy against hepatocellular carcinoma. Hepatol Res. 2018;48(8):597-607.
27. Almendro V, Garcia-Recio S, Gascon P. Tyrosine kinase receptor transactivation associated to G protein-coupled receptors. Curr Drug Targets. 2010;11(9):1169-80.
28. Xu AM, Huang PH. Receptor tyrosine kinase coactivation networks in cancer. Cancer Res. 2010;70(10):3857-60.
29. Chen S, Cao Q, Wen W, Wang H. Targeted therapy for hepatocellular carcinoma: Challenges and opportunities. Cancer Lett. 2019;460:1-9.
30. Wei L, Lee D, Law CT, Zhang MS, Shen J, Chin DW, et al. Genome-wide CRISPR/Cas9 library screening identified PHGDH as a critical driver for Sorafenib resistance in HCC. Nat Commun. 2019;10(1):4681.
31. Sueangoen N, Tantiwetrueangdet A, Panvichian R. HCC-derived EGFR mutants are functioning, EGF-dependent, and erlotinib-resistant. Cell Biosci. 2020;10:41.
32. Lu W, Kang Y. Epithelial-Mesenchymal Plasticity in Cancer Progression and Metastasis. Dev Cell. 2019;49(3):361-74.
33. Hwang HS, Go H, Park JM, Yoon SY, Lee JL, Jeong SU, et al. Epithelial-mesenchymal transition as a mechanism of resistance

to tyrosine kinase inhibitors in clear cell renal cell carcinoma. Lab Invest. 2019;99(5):659-70.
34. Mir N, Jayachandran A, Dhungel B, Shrestha R, Steel JC. Epithelial-to-Mesenchymal Transition: A Mediator of Sorafenib Resistance in Advanced Hepatocellular Carcinoma. Curr Cancer Drug Targets. 2017;17(8):698-706.
35. Cao L, Fan X, Jing W, Liang Y, Chen R, Liu Y, et al. Osteopontin promotes a cancer stem cell-like phenotype in hepatocellular carcinoma cells via an integrin-NF-kappaB-HIF-1alpha pathway. Oncotarget. 2015;6(9):6627-40.
36. Dong Q, Zhu X, Dai C, Zhang X, Gao X, Wei J, et al. Osteopontin promotes epithelial-mesenchymal transition of hepatocellular carcinoma through regulating vimentin. Oncotarget. 2016;7(11):12997-3012.
37. Lei Y, Yan W, Lin Z, Liu J, Tian D, Han P. Comprehensive analysis of partial epithelial mesenchymal transition-related genes in hepatocellular carcinoma. Journal of Cellular and Molecular Medicine. 2021;25:448-62.
38. Zhao H, Chen Q, Alam A, Cui J, Suen KC, Soo AP, et al. The role of osteopontin in the progression of solid organ tumour. Cell Death Dis. 2018;9(3):356.
39. Pan HW, Ou YH, Peng SY, Liu SH, Lai PL, Lee PH, et al. Overexpression of osteopontin is associated with intrahepatic metastasis, early recurrence, and poorer prognosis of surgically resected hepatocellular carcinoma. Cancer. 2003;98(1):119-27.
40. Hirama M, Takahashi F, Takahashi K, Akutagawa S, Shimizu K, Soma S, et al. Osteopontin overproduced by tumor cells acts as a potent angiogenic factor contributing to tumor growth. Cancer Letters. 2003;198(1):107-17.
41. Rittling SR, Chambers AF. Role of osteopontin in tumour progression. Br J Cancer. 2004;90(10):1877-81.
42. Weber GF. The metastasis gene osteopontin: a candidate target for cancer therapy. Biochim Biophys Acta. 2001;1552(2):61-85.
43. Tokuda K, Morine Y, Miyazaki K, Yamada S, Saito Y, Nishi M, et al. The interaction between cancer associated fibroblasts and tumor associated macrophages via the osteopontin pathway in the tumor microenvironment of hepatocellular carcinoma. Oncotarget. 2021;12:333-43.
44. Nallasamy P, Nimmakayala RK, Karmakar S, Leon F, Seshacharyulu P, Lakshmanan I, et al. Pancreatic Tumor Microenvironment Factor Promotes Cancer Stemness via SPP1-CD44 Axis. Gastroenterology. 2021;161(6):1998-2013 e7.
45. Khalil A, Elgedawy J, Faramawi MF, Elfert A, Salama I, Abbass A, et al. Plasma osteopontin level as a diagnostic marker of hepatocellular carcinoma in patients with radiological evidence of focal hepatic lesions. Tumori. 2013;99:100-7.
46. Kim J, Ki SS, Lee SD, Han CJ, Kim YC, Park SH, et al. Elevated plasma osteopontin levels in patients with hepatocellular carcinoma. Am J Gastroenterol. 2006;101(9):2051-9.
47. Zhang H, Ye QH, Ren N, Zhao L, Wang YF, Wu X, et al. The prognostic significance of preoperative plasma levels of osteopontin in patients with hepatocellular carcinoma. J Cancer Res Clin Oncol. 2006;132(11):709-17.

SUPPORTING INFORMATION

Additional supporting information can be found online in the Supporting Information section at the end of this article.

How to cite this article: Eun JW, Yoon JH, Ahn HR, Kim S, Kim YB, Lim SB, et al. Cancer-associated fibroblast-derived secreted phosphoprotein 1 contributes to resistance of hepatocellular carcinoma to sorafenib and lenvatinib. Cancer Communications. 2023;1–25. https://doi.org/10.1002/cac2.12414